PRIMARY RESEARCH ARTICLE

Global Change Biology WILEY

Historical increases in land-derived nutrient inputs may alleviate effects of a changing physical climate on the oceanic carbon cycle

Fabrice Lacroix[1,2,3] | Tatiana Ilyina[2] | Moritz Mathis[4] | Goulven G. Laruelle[3] | Pierre Regnier[3]

[1]Biogeochemical Signals (BSI), Max Planck Institute for Biogeochemistry, Jena, Germany

[2]Ocean in the Earth System (OES), Max Planck Institute for Meteorology, Hamburg, Germany

[3]Biogeochemistry & Modeling of the Earth System, Department Geoscience, Environment & Society (DGES), Université Libre de Bruxelles, Brussels, Belgium

[4]Institute of Coastal Systems Analysis and Modeling, Heimholz-Zentrum Geesthacht, Geesthacht, Germany

Correspondence
Fabrice Lacroix, Biogeochemical Signals (BSI), Max Planck Institute for Biogeochemistry, Jena, Germany.
Email: fabrice.lacroix@mpimet.mpg.de

Abstract

The implications of climate change and other human perturbations on the oceanic carbon cycle are still associated with large uncertainties. Global-scale modelling studies are essential to investigate anthropogenic perturbations of oceanic carbon fluxes but, until now, they have not considered the impacts of temporal changes in riverine and atmospheric inputs of P and N on the marine net biological productivity (NPP) and air–sea CO_2 exchange (FCO_2). To address this, we perform a series of simulations using an enhanced version of the global ocean biogeochemistry model HAMOCC to isolate effects arising from (1) increasing atmospheric CO_2 levels, (2) a changing physical climate and (3) alterations in inputs of terrigenous P and N on marine carbon cycling over the 1905–2010 period. Our simulations reveal that our first-order approximation of increased terrigenous nutrient inputs causes an enhancement of 2.15 Pg C year^{-1} of the global marine NPP, a relative increase of +5% over the simulation period. This increase completely compensates the simulated NPP decrease as a result of increased upper ocean stratification of −3% in relative terms. The coastal ocean undergoes a global relative increase of 14% in NPP arising largely from increased riverine inputs, with regional increases exceeding 100%, for instance on the shelves of the Bay of Bengal. The imprint of enhanced terrigenous nutrient inputs is also simulated further offshore, inducing a 1.75 Pg C year^{-1} (+4%) enhancement of the NPP in the open ocean. This finding implies that the perturbation of carbon fluxes through coastal eutrophication may extend further offshore than that was previously assumed. While increased nutrient inputs are the largest driver of change for the CO_2 uptake at the regional scale and enhance the global coastal ocean CO_2 uptake by 0.02 Pg C year^{-1}, they only marginally affect the FCO_2 of the open ocean over our study's timeline.

KEYWORDS
air–sea CO_2 exchange, coastal budgets, coastal eutrophication, cross-shelf exports, global carbon cycle, marine productivity, ocean stratification, river transport

1 | INTRODUCTION

The intensity of the oceanic carbon uptake partly buffers the increase in atmospheric CO_2 caused by anthropogenic emissions (Friedlingstein et al., 2019; Peters et al., 2017). The carbon uptake through biological productivity and its vertical transfer to the deep ocean is an important pathway of the net air–sea CO_2 exchange (FCO_2, Falkowski et al., 1998; Sabine et al., 2004), although large uncertainties remain associated with its past and potential future efficiency over spatial and temporal scales (Beaulieu et al., 2013; Bopp et al., 2013; Henson et al., 2010; Kwiatkowski et al., 2020; Laufkötter et al., 2015; Maerz et al., 2020).

The ocean's biological productivity is, to a large extent, controlled by light availability and nutrient concentrations, which are dependent on physical characteristics such as ocean circulation, stratification and temperature (Behrenfeld et al., 2006; Falkowski et al., 1998; Holt et al., 2018). These large-scale physical oceanic features have undergone significant alterations during the 20th century due to changes in the Earth's climate and atmospheric circulation (Church et al., 2011; Kuhlbrodt & Gregory, 2012; Rhein et al., 2013). Increased radiative forcing and an enhanced hydrological cycle as responses to anthropogenic greenhouse gas emissions have, for one, led to widespread decreases in upper ocean densities, causing a buoyancy-driven intensification of the permanent stratification of the ocean (Rhein et al., 2013). These physical changes, in turn, could have initiated a disruption of biogeochemical cycling in the biologically active upper ocean. Since increased stratification inhibits the vertical supply of dissolved inorganic nutrients from intermediate ocean layers to the upper ocean, it likely affects the oceanic biological carbon uptake by limiting the net primary productivity (NPP), although the magnitude of this disruption is strongly uncertain at the global scale as demonstrated in the global model studies of Bopp et al. (2013), Laufkötter et al. (2013), Matsumoto et al. (2010) and Kwiatkowski et al. (2017, 2020). Observational studies, based on either in-situ or from satellite data, have furthermore also disagreed with respect to the sign and magnitude of global oceanic NPP changes (Behrenfeld et al., 2006; Saba et al., 2011), which may arise from the short-term variability controlling NPP trends over decadal timescales, as suggested in the modelling studies of Beaulieu et al. (2012) and Henson et al. (2010). These studies have implied that the lengths of currently available NPP observational time-series are too short to conclusively estimate long-term trends.

In addition to the perturbations arising from changes in the physical climate, the global biogeochemical cycles of the essential macro-nutrients nitrogen (N) and phosphorus (P) have also been dramatically disrupted by anthropogenic activities over the past two centuries (Galloway, 1995; Gruber & Galloway, 2008; Stumm, 1973), causing alterations in the aeolian and riverine transports of N and P to the ocean (Doney et al., 2007; Holt et al., 2018; Mahowald et al., 2017; Rabouille et al., 2001; St-Laurent et al., 2017; Ver et al., 1999; Yang & Gruber, 2016). The increased riverine transport of these nutrients from land to ocean has also led to important environmental deterioration in the coastal ocean, such as increased eutrophication, hypoxia and acidification (Bauer et al., 2013; Breitburg et al., 2018; Diaz & Rosenberg, 2008; Fennel & Testa, 2019; Holt et al., 2016; Laurent et al., 2017; Terhaar et al., 2019). These detrimental effects have already been investigated through analysis of observational data (e.g. Diaz & Rosenberg, 2008) as well as through regional models (e.g. Laurent et al., 2017; St-Laurent et al., 2017) at the regional scale, but a global assessment is still withstanding. The perturbation of the transfer of nutrients from land-to-ocean has also likely induced significant changes for the global coastal ocean carbon cycle (Mackenzie et al., 2002; Rabouille et al., 2001; Ver et al., 1999). For instance, conceptual box model studies suggest that increasing riverine nutrient fluxes have altered the net ecosystem productivity (NEP) of the coastal ocean towards autotrophy and stimulated the uptake of anthropogenic CO_2 (Mackenzie et al., 2002; Rabouille et al., 2001; Ver et al., 1999). These responses are however entailed with important uncertainties since box models do not represent the three-dimensional features of the coastal ocean (Lacroix et al., 2021). In contrast, general ocean circulation models, which are typically components of Earth System Models (Aumont et al., 2015; Boucher et al., 2020; Dunne et al., 2020; Jungclaus et al., 2013; Mauritsen et al., 2018; Seland et al., 2020), can now broadly represent circulation features of the continental margins if applied at a high-enough resolution (Jungclaus et al., 2013; Lacroix et al., 2021; Liu et al., 2019). The temporal changes associated with increasing riverine nutrient inputs have, however, been omitted in standard configurations of state-of-the-art Global Ocean Biogeochemical Models (GOBMs) until now (Bopp et al., 2013; Laufkötter et al., 2013, 2015; Matsumoto et al., 2010).

In the present study, we investigate the isolated and combined consequences of increasing atmospheric CO_2 concentrations, a changing physical climate and enhanced terrigenous nutrient inputs on the oceanic NPP and FCO_2 in a GOBM. To achieve this, we perform sequential transient simulations with (1) increasing atmospheric CO_2 levels, (2) changes in the physical climate and (3) perturbations of terrigenous nutrient inputs to the ocean for the time period 1905–2010 while using a version of the GOBM HAMOCC that was enhanced for a better representation of coastal carbon cycling. With this model setup, we address the following questions:

- What is the magnitude of the marine NPP change as a consequence of altered terrigenous P and N inputs to the ocean over the past century and how does this contrast with changes driven by the physical climate?
- How do these nutrient-derived changes in NPP translate into changes in global FCO_2 and how do they compare to those induced by increasing atmospheric CO_2 levels and changes in the physical climate?
- What is the contribution of the coastal ocean to changes in the global oceanic NPP and FCO_2 over the simulated time period?

2 | MATERIALS AND METHODS

2.1 | Overview of the ocean model configuration

To simulate physical and biogeochemical processes in the ocean, we used a model configuration consisting of the ocean general circulation model Max Planck Institute Ocean Model (MPI-OM; Jungclaus et al., 2013; Mauritsen et al., 2019) coupled to a version of the global ocean biogeochemical model HAMburg Ocean Carbon Cycle (HAMOCC, Ilyina et al., 2013; Paulsen et al., 2017) that was enhanced for an improved representation of carbon cycling in the coastal ocean (Lacroix et al., 2020, 2021).

The MPI-OM simulates oceanic circulation, which dictates the transport of biogeochemical tracers through advection and eddy diffusion. In this study, we used an eddy-permitting horizontal resolution of around 0.4° (MPI-OM TP04 configuration, see Jungclaus et al., 2013), which is 2–4 times higher than what has been conventionally used in GOBM studies in global analysis. Although this resolution remains insufficient to accurately represent some of the fine-scale processes taking place in the coastal ocean (Fennel et al., 2006; Gruber et al., 2011; Pätsch et al., 2017), the model setup simulates plausible regional coastal water residence times and distributions of biogeochemical indicators (Lacroix et al., 2021). The atmospheric state used to drive the oceanic physics was obtained from the ERA-20C 20th-century reanalysis (Poli et al., 2016). In this reanalysis product, a coupled atmosphere–land surface–ocean wave model was forced with observational data for sea-ice cover, surface temperature, solar forcing and atmospheric composition changes to assimilate surface pressure and marine wind observations. In our study, we applied the ERA-20C data over the entire simulation period (1905–2010), with 1905 being the earliest year for which a complete dataset is available at a 3-hourly temporal resolution.

The standard version of HAMOCC simulates the main processes that affect the organic and inorganic cycling of carbon and nutrients in the water column and in the sediment, as well as the dynamics of gases in the ocean and their exchanges at the air–sea interface (Ilyina et al., 2013; Lacroix et al., 2021; Mauritsen et al., 2019). The organic carbon cycling module is based on an extended NPZD (Nutrients, Phytoplankton, Zooplankton and Detritus) formulation with the addition of marine dissolved organic matter (Six & Maier-Reimer, 1996), cyanobacteria (Paulsen et al., 2017) and terrigenous dissolved organic matter pools (Lacroix et al., 2020) as additional model tracers. The inorganic pools in HAMOCC include dissolved inorganic phosphorus (DIP), dissolved inorganic nitrogen (DIN), dissolved silica, dissolved iron, dissolved inorganic carbon (DIC), and alkalinity as well as opal and calcium carbonate as particulate constituents. The model also resolves the marine transport and air-sea exchange of CO_2, O_2, N_2 and N_2O gases.

HAMOCC was extended with prescribed pre-industrial riverine inputs of carbon, alkalinity, P, N, silica and iron, along with their speciation as described in Lacroix et al. (2020), which we use here to initialize the pre-industrial state of the model. Due to likely underestimations of riverine carbon inputs in Lacroix et al. (2020), we use the higher tDOM inputs of 0.24 Pg C year^{-1}, as is described in Lacroix et al. (2021). Furthermore, the coastal sedimentary Particulate Organic Matter (POM) degradation rate constant was increased (water depth <250 m) to 0.0026 day^{-1}, in contrast to the 0.001 day^{-1} rate applied in the open ocean, to capture the generally higher rates of organic matter decomposition reported for shallow marine environments as shown in Lacroix et al. (2021).

In addition to riverine inputs, the model accounts for additional inputs of nitrogen to the ocean originate via N-fixation through cyanobacteria (Paulsen et al., 2017) and atmospheric deposition as given by a climatological flux field of Doney et al. (2007) for 1850–1905 for the pre-industrial timeframe. Iron is added to the model following a spatially resolved climatological dust deposition flux field, as described in Mahowald et al. (2005).

2.2 | The anthropogenic perturbation of nutrient inputs to the ocean

The changes of riverine P and N exports to the ocean over the 1905–2010 period were derived using data from the Global-NEWS2 study (Mayorga et al., 2010; Seitzinger et al., 2010), which is an established spatially explicit statistical model that was developed to produce hindcast and future scenarios of yearly averaged, global riverine nutrient exports to the ocean. These changes in nutrient inputs over 1905–2010 were prescribed to the ocean biogeochemical model on top of the prescribed pre-industrial riverine loads as estimated for the year 1905 (described in detail in Lacroix et al., 2020), the beginning of our transient simulations.

We used the simulated NEWS2 anthropogenic components of DIP and DOP loads to estimate anthropogenic perturbations of riverine P inputs, and of DIN and DON to estimate anthropogenic perturbations of riverine N inputs for the year 2000, which are all explicitly quantified in the Global-NEWS2 run5 c00 simulation (Seitzinger et al., 2010). To estimate the temporal evolution of the P and N increase over the timespan, we constructed a global temporal evolution of the anthropogenic P and N loads similar to the model results of Beusen et al. (2016). The global riverine P and N rise was relatively weak between 1900 and 1925, followed by a fourfold faster increase over the 1925–2000 period (Figure 1a–d). For N loads, results from the Beusen et al. (2016) show that the increase might be even steeper and nonlinear from 1975 onwards. For the period 2000–2010 that was investigated in more detail by Seitzinger et al. (2010), we averaged over their 'business-as-usual' scenario (CI, same increase in riverine P and N loads as for 1925–2000; Figure 1), and two contrasting scenarios from Global-NEWS2 that consider distinct agricultural policy and water management strategies (the Global Orchestration (GO) and Adapting Mosaic (AM) trajectories). These first-order linear estimations of temporal dynamics of riverine loads imply some limitations for our study, which we discuss in Section 5. Since we focus on long-term, century-scale trends here, we believe these temporal patterns likely have only minor effects on the results presented here for the global scale.
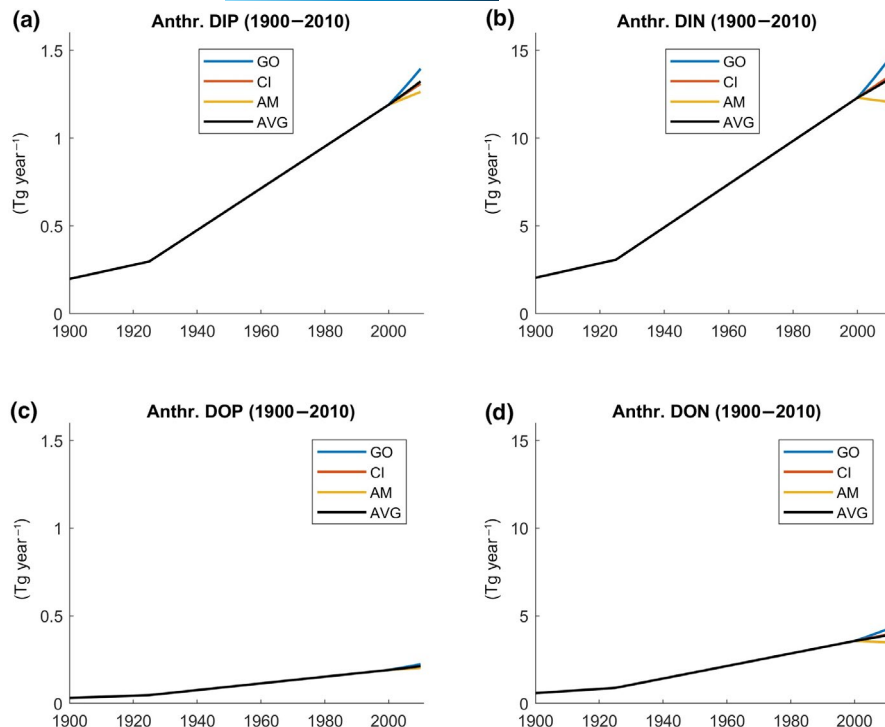
FIGURE 1 Evolution of global anthropogenic riverine (a) DIP, (b) DIN, (c) dissolved organic phosphorus (DOP) and (d) dissolved organic nitrogen (DON) loads [Tg year^{-1}] as derived in our study

The computed mean annual riverine inputs were injected at their river mouths homogeneously over the course of the year, thus ignoring the intra-annual variability in anthropogenic P and N riverine loads. Furthermore, we assumed that the anthropogenic DOP and DON is highly reactive and easily bioavailable in the coastal ocean due to the increased quality of tDOM with higher relative N and P contents (Lønborg & Álvarez-Salgado, 2012). Therefore, the riverine exports of these organic species were also added to the DIP and DIN pools in HAMOCC.

In the Global-NEWS2 study, particulate P and N were suggested to remain approximately constant compared to pre-industrial riverine inputs over the simulation timescale, and therefore, particulate loads in our model were assumed to remain constant over the 1905–2010 period.

In addition to riverine inputs, we considered increased atmospheric N deposition inputs from 1905 to 2010 constructed from the dataset of Doney et al. (2007).

2.3 | Model initialization and experiment design

Taking into account the long timescales of the marine carbon cycle feedbacks, we initialized the 1905–2010 model simulations in a way that minimizes trends of model variables arising from previous disequilibrium of the model. This was realized using a three-step procedure. First, we performed a model simulation over 1000 years using its complete configuration, thus using all MPIOM-HAMOCC modules. Secondly, to reduce computing cost associated with the initialization of the sediment module (Heinze et al., 1999), an average of the particulate fluxes from the last 10 years of the above simulation was extracted to drive the sediment module in standalone mode for
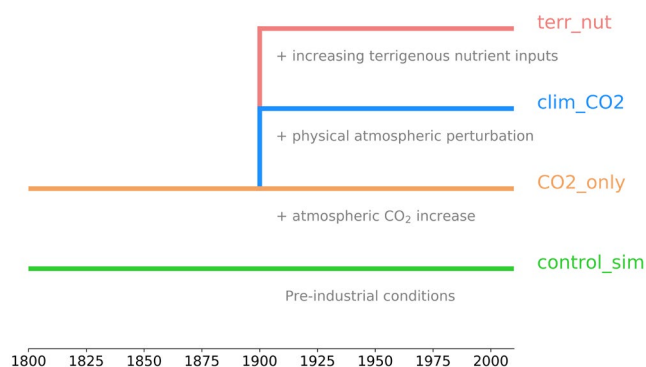
FIGURE 2 Summary of the simulation strategy

10,000 years. Thirdly, the resulting sediment state was coupled back to the water column, and the full MPIOM-HAMOCC configuration was run again for another 1000 simulation years. During the initialization, the ocean circulation of MPIOM was driven by the ERA20C dataset repeatedly over the timeframe 1905–1930 to represent pre-industrial conditions as closely as possible from the available dataset.

Once the initialization was completed, we performed four transient simulations to isolate the effects of three individual drivers of the marine carbon cycle perturbations (Figure 2). We first performed two simulations from 1800 to 2010: control_sim and CO2_only. The simulation control_sim was carried out at pre-industrial atmospheric conditions, and was only used as a reference simulation to check for any remaining model drifts. Simulation CO2_only accounts for the increase in atmospheric CO_2 concentrations from 278 to 389 ppm over the 1800–2010 period (Etheridge et al., 1996), while still being driven by the prescribed pre-industrial physical climate state and riverine loads. We then performed two additional simulations starting

at year 1905 of *CO2_only*, which were carried out until 2010. The first of these simulations, *clim_CO2*, accounts for changes in the physical climate forcing of the ocean as constrained by the atmospheric ERA-20C 1905–2010 forcing in addition to the changes in atmospheric CO_2 concentrations over the time period. The second simulation, *terr_nut*, accounts for perturbations in riverine and atmospheric deposition inputs of P and N over 1905–2010, as described above, in addition to changes in atmospheric CO_2 concentrations and of the physical climate, thus all perturbations combined.

2.4 | Analysis strategy

To evaluate our results in the context of contemporary observational datasets and estimates, we averaged the final 20 years (i.e. over 1990 to 2010) of the simulation *terr_nut*, which accounts for all perturbations. We computed trends in nutrient concentrations and NPP through linear regressions over the entire 1905–2010 period. The significance of the regressions was tested through Student's *t* tests for $p < 0.05$. The evolution of the FCO_2 over the investigated time span, however, was clearly not linear in our study due to the acceleration in the increase in atmospheric CO_2 throughout the 20th century. We therefore compared temporal means for 1890–1910 with temporal means for the 1990–2010 period to quantify the effects of the different perturbations on the change in FCO_2 in order to reduce effects of decadal variability.

We decomposed effects arising from increasing atmospheric CO_2 levels, *CO2-induced*, by subtracting *control_sim* from *only_CO2*. Hydrodynamical and biogeochemical perturbations arising from the changes in the physical climate, *climate-induced*, were estimated by subtracting *only_CO2* from *clim_CO2*. Biogeochemical perturbations from increasing terrigenous P and N inputs, both from atmospheric deposition and riverine runoff, *terr. nut-induced*, were quantified by subtracting *clim_CO2* from *terr_nut*.

Note that *control_sim* and *CO2_only* do not differ significantly in terms of global nutrient concentrations and oceanic NPP, since the drivers of biological productivity in the two simulations remain essentially the same, except for small model drifts. We therefore use the *CO2_only* experiment as reference in our analysis of temporal changes in surface nutrient concentrations and NPP.

2.5 | Segmentation of the open and coastal ocean

In our analysis, we differentiate between the responses of the open and coastal ocean to the different anthropogenic perturbations. Definitions of the boundary between coastal and open ocean vary considerably in the literature (Chen & Borges, 2009; Laruelle et al., 2013, 2014, 2017, 2018; Muller-Karger et al., 2005). In our analysis, we used a simple depth-dependent coastal ocean threshold of 250 m, which is in consistency with Lacroix et al. (2021). This definition is more inclusive than the often used 200 m isobath limit (Chen & Borges, 2009), with the goal to include numerous shelves

that extend significantly further than 200 m, such as Arctic Ocean shelves (Laruelle et al., 2013). The depths of the seafloor in the model originate from modification and interpolation of the ETOPO2 bathymetry (NOAA National Geophysical Data Center, 2006) for the MPIOM TP04 model grid configuration (Jungclaus et al., 2013).

In addition to this, we differentiated between shelf regions of the Pacific, Atlantic, Indian and Arctic basins to perform a high-level regional analysis of the various perturbations while also delineating in terms of northern and southern mid-latitude shelves (from 23.5 to 60° of both southern and northern hemispheres, respectively), as well as tropical shelves (from 23.5°S to 23.5°N, Figure S1a). To analyse the differences between individual regions at a finer-scale, we also selected three shelf regions (eastern North America, East China Sea and Sunda shelf) that are reported to be to a large part driven by open ocean inflows, as well as three other regions (southern North Sea, Louisiana Shelf and Bay of Bengal shelves), where riverine perturbations are thought to have a larger impact on the aquatic biogeochemistry (Figure S1b).

3 | RESULTS

3.1 | Perturbations of riverine and atmospheric deposition of P and N inputs to the ocean

Our calculations that combine data from Lacroix et al. (2020) and the Global-NEWS product indicate an increase in the global riverine DIP export to the ocean from 0.5 Tg P year^{-1} in 1905, with 0.2 Tg P year^{-1} already being of anthropogenic origin, to 1.6 Tg P year^{-1} in 2010. We also estimate an increase in the global riverine DIN load from 3.6 Tg N year^{-1} (2.1 Tg N year^{-1} of anthropogenic origin) to 17.1 Tg N year^{-1} over the same period. Changes in dissolved organic P and N loads are less pronounced in absolute magnitudes, with global riverine DOP and DON loads increasing from 0.1 to 0.4 Tg P year^{-1} and 1.5 to 5.4 Tg N year^{-1}, respectively. Biologically available riverine P (DIP and DOP) and N (DIN and DON) loads are therefore projected to have undergone significant increases of around 1.4 Tg P year^{-1} (+233%) and 17 Tg N year^{-1} (+349%) over the simulation period. When also accounting for particulate P and N loads, total global riverine P and N loads increase from 3.7 to 5.3 Tg P year^{-1} (+43% increase) and from 27 to 46 Tg N year^{-1} (+70% increase), respectively. Our global riverine P and N exports to the ocean are, therefore, comprised within the previously estimated range for the pre-industrial time period of 2–4.5 Tg P year^{-1} (Beusen et al., 2016; Compton et al., 2000) and 14–21 Tg N year^{-1} (Beusen et al., 2016; Green et al., 2004), and within the estimated range of 4–21 Tg P year^{-1} for and 36–60 Tg N year^{-1} for the present day (Beusen et al., 2016; Bouwman et al., 2005; Green et al., 2004; Lee et al., 2019; Meybeck, 1982; Seitzinger et al., 2010; Van Drecht et al., 2005). The N:P mole ratio of the estimated anthropogenic increase is 19:1 over the 1905–2010 period, which is slightly higher than the Redfield N:P ratio of 16:1, the classically assumed ratio of organic matter production in the ocean (Takahashi et al., 1985).

At the ocean basin scale, the largest relative increases in global P and N loads take place in the Indo-Pacific (+39% P, +44% N) while the Atlantic also exhibits a large perturbation (+28% P and +29% N). The Ganges, providing increased inputs of 0.1 Tg P year^{-1}, 1.40 Tg N year^{-1} to the Indian basin (Table 1), shows by far the largest perturbation, with changes in this catchment's biogeochemical characteristics also reported in literature (Sattar et al., 2014). Increased P and N inputs to the western Pacific Ocean (Figure 3a,b) are mainly attributed to Southeast Asian catchments being affected by increased riverine P and N inputs originating from agriculture and sewage (Wang et al., 2015). The riverine inputs to the tropical Atlantic are also estimated to have strongly increased due to enhanced transports from the Amazon and Congo rivers (Table 1). Additionally, rivers discharging onto the North Atlantic shelves show a strong degree of perturbation (Figure 3a,b), confirming increased nutrients on these shelves documented as early as the 1970s (Radach & Pätsch, 2007; Van Bennekom et al., 1975). The Mississippi river is another catchment that has undergone strong anthropogenic disturbances (Fennel & Testa, 2019; Laurent et al., 2017; Rabalais et al., 2002), with increases reaching 0.032 Tg P year^{-1} and 0.23 Tg N year^{-1} according to our framework. The P and N loads from Arctic rivers only change marginally over the simulation period according to Global-NEWS2, with large watersheds such as the Lena or the Mackenzie rivers remaining in nearly pristine conditions, a result in agreement with those of Beusen et al. (2016), although it should be noted that changes induced by permafrost thawing are not included in both studies.

In addition to enhanced oceanic nutrient inputs from riverine loads, we consider global atmospheric N deposition to contribute to an additional increase in N inputs to the ocean, increasing from 14.6 Tg N year^{-1} in 1905 to 20.9 Tg N year^{-1} in 2009 (Doney et al., 2007). Out of this 6.3 Tg N year^{-1} increase, 1.4 Tg N year^{-1} is deposited to the coastal ocean. Spatially, the strongest increases in N deposition fluxes occur in the North Atlantic, as well as in the West Pacific off the Asian continent (Figure 3b).

3.2 | Contemporary (1990–2010) ocean variables evaluated against observational data

The 1990–2010 global mean sea surface temperature (SST) of 17.7 ± 0.8°C in the *terr_nut* simulation is in good agreement with the global World Ocean Atlas 2018 (WOA18, Boyer et al., 2018) mean value of 18.2 ± 1.7°C over 1981–2010. The spatial distribution of observed SST is also well captured in the model (Figure S2a,b).
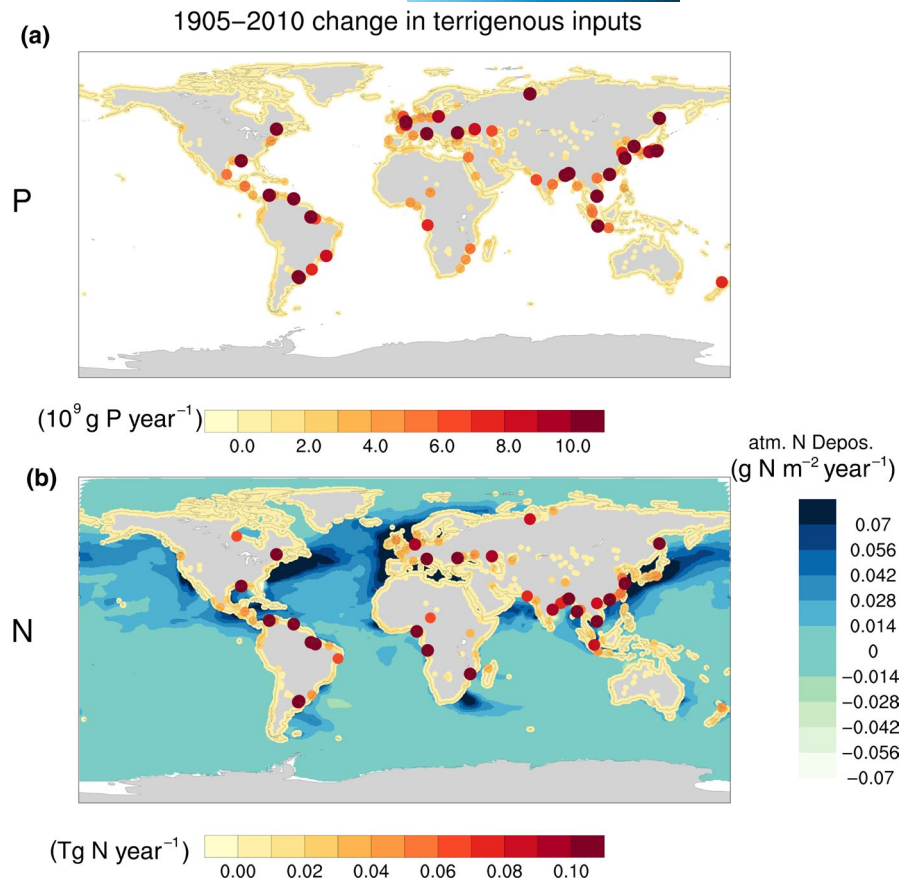
The present-day global annual mean surface nutrient concentrations, which accounts for approximately the first 10 m of ocean water depths, are 0.37 ± 0.01 μM DIP and 4.61 ± 0.01 μM DIN in *terr_nut*. These values are comparable to those derived from the WOA18 observational data (0.47 ± 0.08 μM DIP and 5.04 ± 0.01 μM DIN). The simulation also captures the observed spatial patterns of dissolved inorganic nutrient concentrations reasonably well (Figure 4a–d). Distributions of DIP and DIN, as well as their biases with respect to global observational datasets, have been extensively discussed in previous studies that used the standard HAMOCC model (Ilyina et al., 2013; Paulsen et al., 2017). Further validation in the context of the implementation of pre-industrial riverine fluxes in HAMOCC can also be found in Lacroix et al. (2020), and the inclusion of the temporal dynamics of terrigenous P and N inputs here only marginally modifies the overall oceanic concentration patterns reported previously (Figure 4e,f). A substantial bias in the model version is the

TABLE 1 Comparison of our model-derived DIP and DIN river loads against published values from the literature for 10 of the largest rivers in terms of freshwater discharge (Seitzinger et al., 2010)
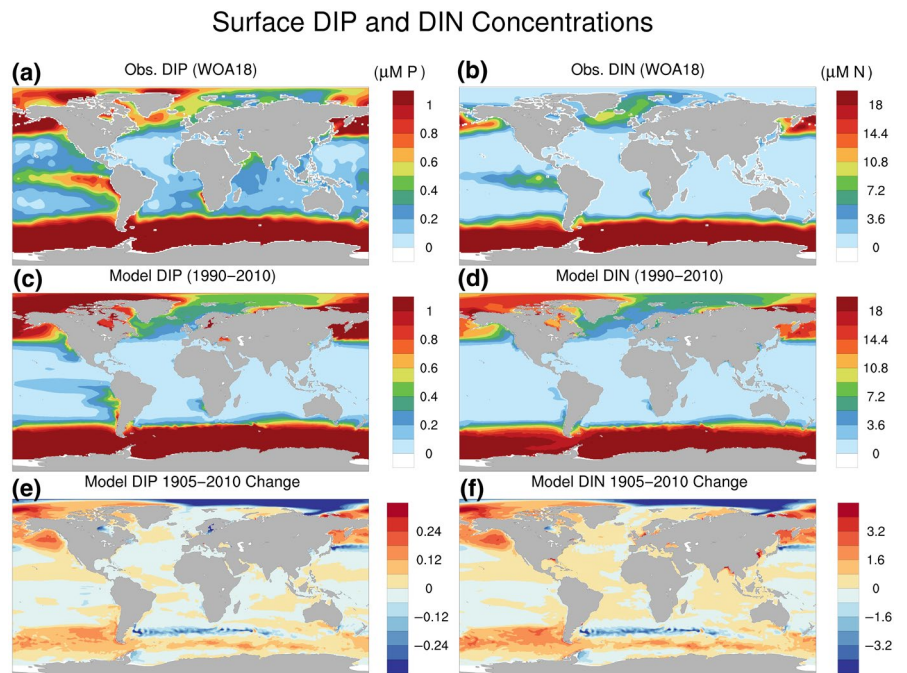
Rivers	DIP load (our study) 10⁹ g P year⁻¹		DIP load (literature) 10⁹ g P year⁻¹	DIN load (our study) Tg N year⁻¹		DIN load (literature) Tg N year⁻¹
	1905	2010	Present day	1905	2010	Present day
Amazon[1]	73	103	221	0.53	0.89	1.09
Congo[2]	2.3	9.4	18	0.02	0.19	0.16
Ganges-Brahmaputra[3]	21	124	165	0.17	1.57	0.95
Yangtze[4]	30	73	92	0.22	1.04	0.78
Yenisei[5]	8.8	10.4	7.9	0.06	0.09	0.16
Lena[5]	8.2	8.5	4.4	0.06	0.06	0.17
Mississippi[6]	16	48	19.5	0.12	0.35	0.79
Mekong[7]	7.2	20	0.9	0.05	0.25	0.29
Ob[5]	14.1	28	20.4	0.1	0.19	0.05
Mackenzie[5]	6.0	6.0	1.5	0.04	0.04	0.06
Global	0.5×10^3	1.6×10^3	$0.5–1.4 \times 10^{3}$ [8,9]	3.6	17.1	16.2–18.9 [9,10]

Note: References: DIP loads from Harrison et al. (2010); DIN loads from [1]Martinelli et al. (2010); [2]Peierls et al. (1991); [3]Whitehead et al. (2015); [4]Shuiwang et al. (2000); [5]Le Fouest et al. (2013); [6]Sprague et al. (2011); [7]Liljeström et al. (2012); [8]Compton et al. (2000); [9]Seitzinger et al. (2010); [10]Turner et al. (2003).

1905–2010 change in terrigenous inputs

(a)

P

$(10^9 \, \text{g P year}^{-1})$

0.0   2.0   4.0   6.0   8.0   10.0

(b)

N

atm. N Depos.
$(\text{g N m}^{-2} \text{ year}^{-1})$

0.07
0.056
0.042
0.028
0.014
0
−0.014
−0.028
−0.042
−0.056
−0.07

(Tg N year^{-1})

0.00   0.02   0.04   0.06   0.08   0.10

Surface DIP and DIN Concentrations

(a) Obs. DIP (WOA18) $(\mu M \, P)$

1
0.8
0.6
0.4
0.2
0

(b) Obs. DIN (WOA18) $(\mu M \, N)$

18
14.4
10.8
7.2
3.6
0

(c) Model DIP (1990–2010)

1
0.8
0.6
0.4
0.2
0

(d) Model DIN (1990–2010)

18
14.4
10.8
7.2
3.6
0

(e) Model DIP 1905–2010 Change

0.24
0.12
0
−0.12
−0.24

(f) Model DIN 1905–2010 Change

3.2
1.6
0
−1.6
−3.2

overestimation of nutrient concentrations in the Arctic (Lacroix et al., 2020). Since P and N riverine inputs to the region are assumed to have remained approximately constant during the 20th century (Seitzinger et al., 2010); this region is, however, not a strong area of focus in our study.

The model simulates a mean global NPP of 48.1 ± 1.1 Pg C year^{-1} for the present day, which is in good agreement with global estimates of 42–56 Pg C year^{-1} based on satellite-derived products (Carr et al., 2006; Field et al., 1998; Muller-Karger et al., 2005) as well as previous global model applications yielding values in the 45–50 Pg C year^{-1} range

(e.g. Lacroix et al., 2020; Paulsen et al., 2017). Other key biological indicators are also relatively well reproduced with respect to observation-based estimates (Table S1). Furthermore, the 1990–2010 mean oceanic sink of atmospheric CO_2 amounts to 1.5 ± 0.2 Pg C year^{-1}, which is comparable to recent estimates of between 1 and 2 Pg C year^{-1} for the same time period (Landschützer et al., 2016).

The addition of terrigenous P and N input perturbations during the 1905–2010 period leads to a strong increase in simulated surface DIP and DIN concentrations in individual coastal regions (Figure 5a–f), which also drastically increases the regional NPP (Figure 5g–i). The regions presented here (Bay of Bengal, Louisiana Shelf and Southern North Sea) are regions where important increases in eutrophication have been reported in literature (Fennel & Testa, 2019). Since our model is limited in its representation of the coastal ocean due to its relatively coarse spatial resolution, DIP and DIN concentrations in these regions are expectedly not in complete agreement with values found in literature. These caveats of our study are further discussed in Section 4.3, where we reflect on the role of the coastal ocean in the overall marine carbon cycle. Our model, by explicitly representing the increasing terrigenous P and N inputs, however diminishes the bias in DIN and DIP concentrations in these regions for the contemporary period.

Simulated coastal water residence times (CWRTs, Figure 6a) compare relatively well to observations, with six out of eight simulated regional CWRTs falling within the observational range, confirming that the MPIOM-TP04 grid configuration used here reproduces CWRTs reasonably well at the global scale (Lacroix et al., 2021).

Nine out of 14 simulated regionalized FCO$_2$ flux densities are also in agreement with observational ranges (Figure 6b), albeit we note that the spread in the regional observational values is often very large. Additionally, we observe an overall good spatial agreement between the simulated pCO$_2$ distribution and the one generated by the neural network interpolation approach of Laruelle et al. (2017; Figure 6c,d).

3.3 | Physical climate-induced changes in SST and Mixed Layer Depth (MLD) over 1905–2010

The ERA-20C reanalysis data, which is used as atmospheric forcing to drive the oceanic circulation here, reveals an increase in the global near-surface air temperature of around 1°C between 1905 and 2010 (Table 2, including land and ocean), determined here via linear trend calculation. The ocean responds to these *climate-induced* perturbations with an increase in global SST of a lower magnitude (~0.4°C over the same period), which is in line with the range of values previously reported in published literature (0.2–0.5°C increase for the upper 100 m of the ocean over the last 50 years according to Levitus et al. (2005) and Rhein et al. (2013). The simulated spatial SST changes are very variable, with increases exceeding 1°C locally (Figure 7a) while other regions actually present an SST decrease over the analysis period. The aggregated oceanic surface warming trend is simulated to be the strongest in the tropics (+0.37°C for 0–23°), subtropics (+0.33°C for 23–35°) and mid-latitudes (+0.77°C for
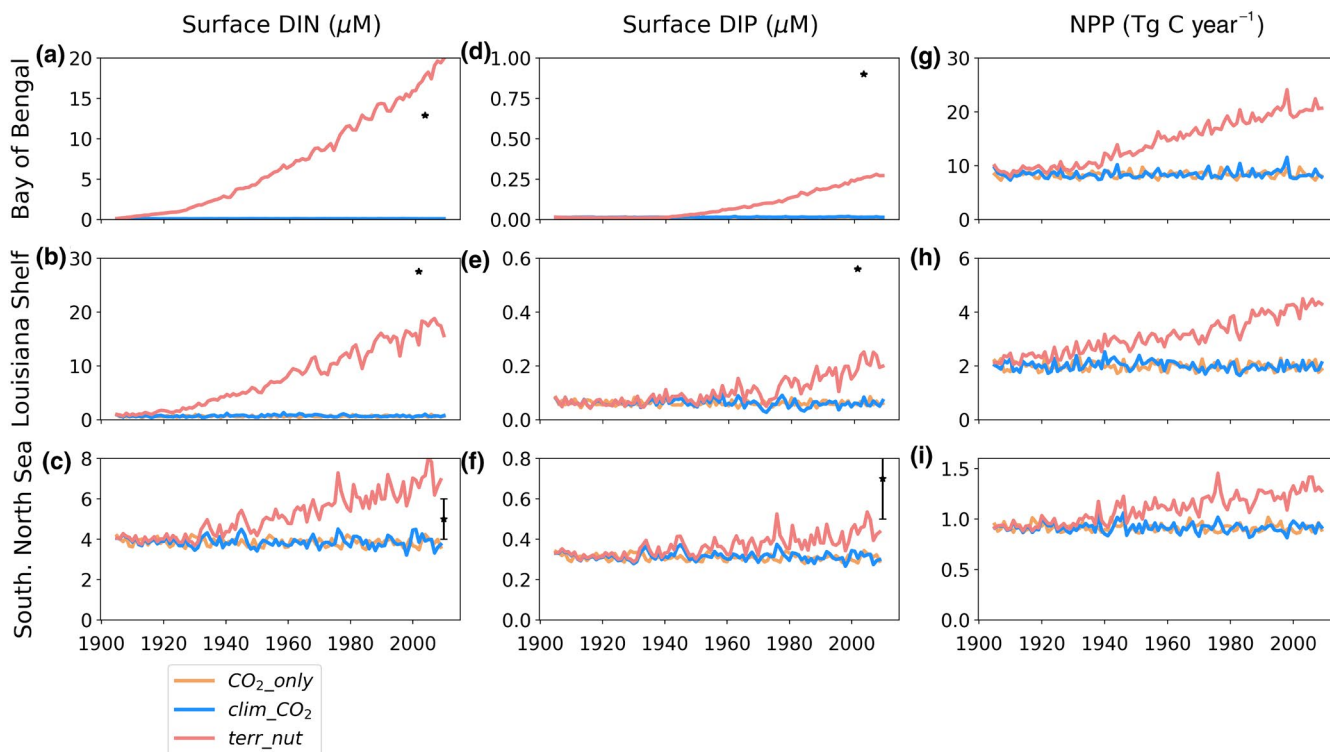
FIGURE 5 Simulated temporal changes in spatially averaged surface DIN (a–c), surface DIP (d–f) and NPP (g–i) in the Bay of Bengal, Louisiana Shelf and Southern North Sea over 1905–2010. The * corresponds to spatially averaged observational data points for the Bay of Bengal (Das et al., 2017), the Louisiana Shelf (Sylvan et al., 2006) and the Southern North Sea (OSPAR, 2017) along with their error bars, if available
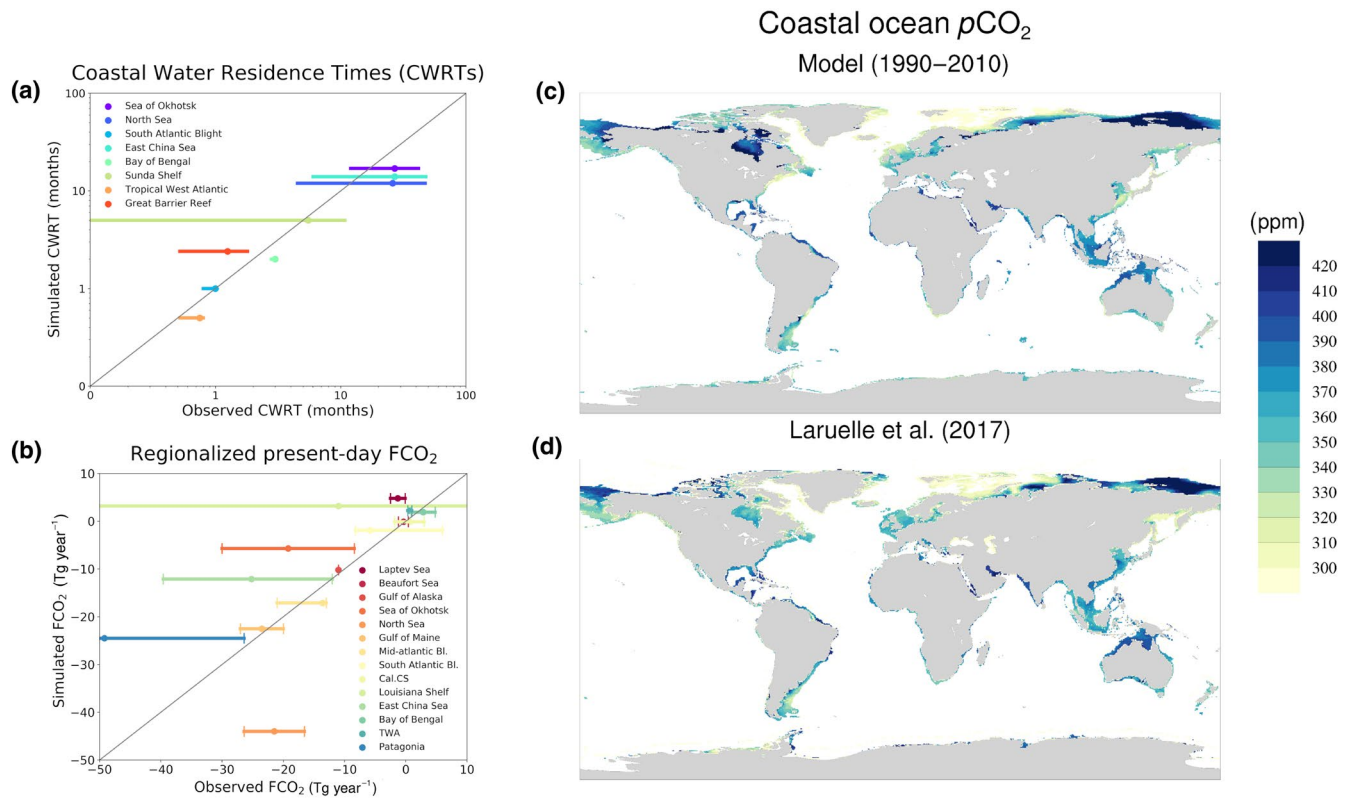
FIGURE 6 Regional-scale comparison of simulated (*terr_nut*, 1990–2010 period) against contemporary observation or regional model-based annual mean estimates of Coastal Water Residence Times CWRT [months] (a) and present-day FCO_2 [Tg C year^{-1}] (b). References for data points in panels (a) and (b) are available in Table S2. In panel (b), a positive flux corresponds to a source to the atmosphere. Panels (c) and (d) compare simulated (*terr_nut*, model 1990–2010 period) global coastal annual mean pCO_2 distribution with the observation-based pCO_2 climatology of Laruelle et al. (2017; annual mean for 1998–2015 period), respectively

TABLE 2 Modelled SST trend over 1905–2010, averaged 1990–2010 SST, modelled MLD temporal trend over 1905–2010 and averaged 1990–2010 MLD for the *terr_nut* simulation. Temporal trends and 1990–2010 averaged values are also provided for the MLD during the winter period (both hemispheres combined). Only trends with statistical significance at $p < 0.05$ are reported

|	1905–2010 SST trend [°C]	1990–2010 mean SST [°C]	1905–2010 MLD trend [m]	1990–2010 mean MLD [m]	1905–2010 winter MLD trend [m]	1990–2010 Winter average MLD [m]
Global Ocean	0.4	17.8 ± 0.8	−19	95	−40	148
Open Ocean	0.4	18.2 ± 0.8	−21	101	−44	153
Coastal Ocean	0.5	14.8 ± 0.3	—	34	—	80

35–66°). In contrast, the trend is weak in the higher latitudes (>66°), with increases of 0.16 and 0.10°C in the Arctic and Southern Oceans on average over the simulation period, respectively.

The simulated mean annual MLD decreases by 19 m globally over 1905–2010 (Table 2). This annual mean decrease is mainly driven by a decrease in the winter-time MLD, when oceanic layers show permanent stratification (considering June–August and December–February as winter in the Southern Hemisphere and in the Northern Hemisphere, respectively). During this season of particular importance for the re-supply nutrients to the euphotic zone, the MLD decreases by 42 m globally over the simulation period globally. In contrast, the summer-time mean MLD of around 31 m (considering December–February and June–August as summer in the southern hemisphere in the northern hemisphere, respectively) is not statistically significantly altered over the simulation period.

Spatially, our model simulates both increasing and decreasing MLDs in many regions over the simulation period (Figure 7b), that sometimes, but not always follow local trends in SST. The averaged MLD in mid-latitudes decreases by 35 m on average over all seasons, mirroring the SST trend of the latitudinal band. The tropics and sub-tropics, which have a strong baseline stratification, show very small decreases in the average MLD of 1 and 2 m, respectively. In contrast, increasing MLDs are simulated in the North Atlantic, parts of the Southern Ocean and in the Arctic, all regions of high complexity with respect to their circulation patterns.

In the global coastal ocean, we simulate an annual mean increase of 0.5°C in the SST over 1905–2010, a warming trend that is practically indistinguishable from the trend for the whole ocean. Surprisingly, our analysis does not reveal a statistically significant decrease in the annual

Change over 1905–2010
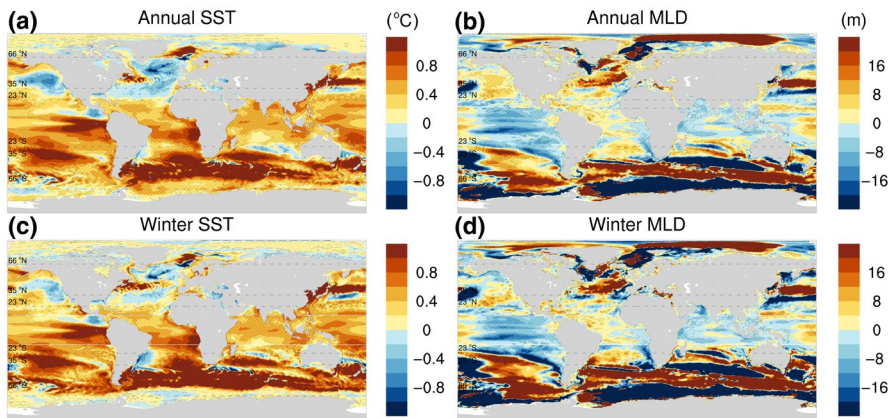
FIGURE 7 Simulated trends in (a) annual mean and (c) winter-time mean sea surface temperatures (SSTs) and (b) annual mean and (d) winter-time mean mixed layer depths (MLDs) induced by *climate-induced* perturbations over the 1905–2010 period, derived via linear trend analysis. Dashed lines show areas with a statistically significant trend (*p* < 0.05)

1905–2010 changes in surface DIP and DIN concentrations
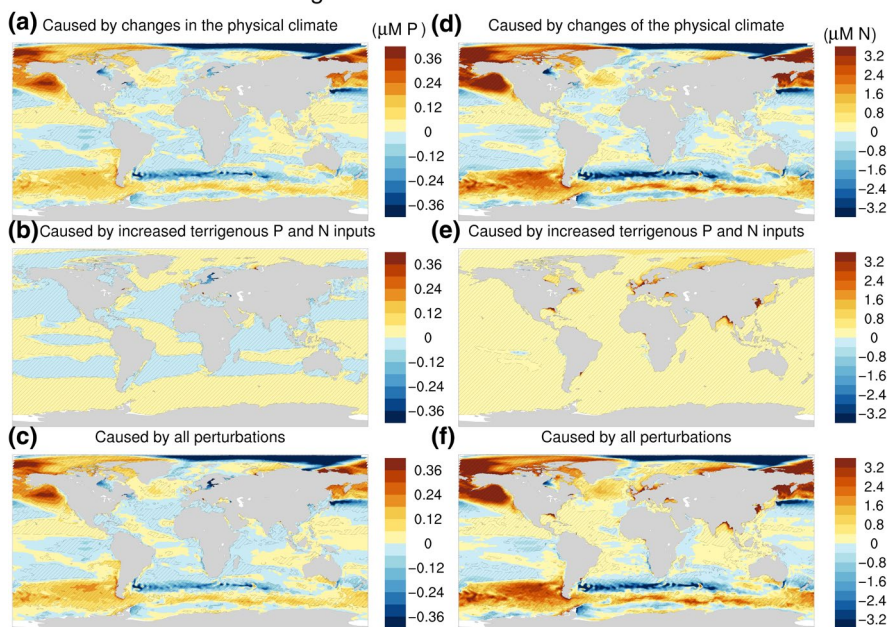
FIGURE 8 Simulated changes in annual mean surface (upper 12 m) ocean DIP/DIN concentrations as a result of (a/d) changes in the physical climate (*climate-induced* perturbations), (b/e) changes in terrigenous nutrient inputs (*terr. nut-induced*), and (c/f) their combined changes over the 1905–2010 period. Dashed areas represent areas where trends are statistically significant at *p* < 0.05

mean coastal MLD, globally. This is likely due to the winter-time MLDs of coastal waters already reaching the sea floor in many regions, since we simulate a global winter-time mean MLD of 80 m in contrast to the shelf sea floor depth of 89 m on average. Despite the non-significant global coastal MLD trend, we observe strong local trends in coastal MLDs annually and in the winter-time (Figure 7b,d). For instance, a strong decrease in winter-time MLD of up to 20 m is simulated on south-western African shelves, whereas we simulate a slight increase in MLD in the East China Sea, despite the winter-time SST increase simulated in the region.

3.4 | Resulting changes in surface nutrient concentrations and oceanic biological productivity

Due to *climate-induced* perturbations, surface ocean global mean N and P concentrations decrease by 0.12 μM N and 0.07 μM P over the 1905–2010 period, accounting for combined total organic and

inorganic N and P inventories. As a result of the same *climate-induced* perturbations, DIN and DIP concentrations, however, surprisingly slightly increase at the global scale (+0.19 μM N and +0.04 μM P), although the global increase is driven by local changes in large parts of the Southern Ocean and the North Pacific (Figure 8a–d), where strong seasonal variability may prevent the efficient use of nutrients made available through complex changes in circulation patterns. In turn, the tropics, subtropics and mid-latitudes largely undergo decreases in surface DIN and DIP concentrations. The *terr. nut-induced* changes cause increases in both total N and P globally (+0.17 μM N and +0.09 μM P). While DIN concentrations rise by 0.09 μM over 1905–2010 on average due to *terr. nut-induced* perturbations, DIP surface concentrations surprisingly decrease (−0.003 μM) at the global scale. The global surface ocean increase in DIN and decrease in DIP is also reflected in global coastal ocean means (changes of +0.7 μM N DIN and −0.5 μM DIP, respectively), suggesting a strengthening in DIP limitation in the model due to

larger relative increases in terrigenous N inputs with respect to P inputs. Decreasing surface DIP concentrations are indeed found in the Western Pacific, the Indian basin and the North Atlantic, basins which undergo a strong degree of perturbation of N inputs from both river transports and atmospheric deposition (Figures 3b and 8b,e). In terms of total changes, thus as a result of *climate-induced* and *terr. nut-induced* perturbations combined, surface concentrations DIN and DIP both slightly increase (+0.24 μM N and +0.01 μM P, respectively). However, both strong increasing and decreasing trends in DIN and DIP are simulated locally as a result of all perturbations (Figure 8c,f).

We also approximate that the net cross-shelf export of inorganic and organic P and N combined are increased by 0.4 and 12 Tg year^{-1} for P and N, respectively (Figures S3 and S4), largely resulting from increased riverine inputs to the coastal ocean.

The *climate-induced* changes cause a statistically significant global NPP decrease of 1.14 Pg C year^{-1} in the model (Figures 9a,d and 10a), corresponding to a decrease of around 3% over the 1905–2010 period. This *climate-induced* decline is of 1.19 Pg C year^{-1} in the global open ocean, whereas the global coastal ocean NPP does not show significant changes. Regionally, negative NPP trends are simulated in the eastern Equatorial Pacific and Pacific subtropical gyres while positive NPP trends are mostly simulated in coastal upwelling regions (e.g. the Benguela Current System), the Southern Ocean, the western Equatorial Pacific and the North Pacific (Figure 11a).

Terr. nut-induced changes cause a significant global oceanic annual mean NPP increase of 2.15 Pg C year^{-1} in our model (Figures 9a,d and 10a), which translates into a relative NPP increase of around 5% for the 1905–2010 period. The increase is stronger in magnitude at low latitudes (Figure 11b), where light limitation of biological primary productivity is less prevalent than at high latitudes. Higher nutrient inputs thus enable an efficient enhancement of phytoplankton growth there. The coastal ocean is directly responsible for a substantial part of the enhanced NPP signal (+0.40 Pg C year^{-1}). Indeed, the relative NPP increase reaches 14% there, being larger than the relative NPP increase in the open ocean (+4%), although the latter undergoes a larger increase in absolute magnitude (+1.75 Pg C year^{-1}). In some parts of the coastal ocean, regional NPP increases exceed 80 g C m^{-2} year^{-1} (Figure 11b), and a doubling of the coastal NPP is simulated regionally over the simulation period. NPP increases in the open ocean are generally much weaker per surface area, but a disproportionate enhancement of the NPP is still simulated in parts of the open ocean, such as in the Tropical Atlantic and Indian Ocean basins, as well as in the Caribbean Sea.

The *climate-induced* and *terr_nut* perturbations of the global oceanic NPP nearly completely counteract each other at the global scale (Figure 10a), leading to a non-significant global NPP trend overall. Our results, however, show a significant positive NPP trend in the global coastal ocean due to the strong perturbation of nutrient inputs there. The model also simulates strong regional trends, both increasing and decreasing, in large parts of the open ocean (Figure 11c).

Despite the substantial decrease/increase in NPP caused by *climate-induced/terr. nut-induced* changes, vertical exports of organic matter are minorly perturbed over the simulation period. We only compute a slight global ocean increase in vertical organic matter export at 90 m depth as a result of *terr. nut-induced* perturbations (+0.06 Pg C year^{-1}), whereas *climate-induced* perturbations do not cause a significant change in the organic matter export at 90 m in our simulations. Due to *terr. nut-induced* perturbations, the coastal ocean experiences a statistically significant increase in POM deposition to the sediment (+0.04 Pg C year^{-1}) and in POM burial (+0.01 Pg C year^{-1}). In contrast, the horizontal export of organic carbon from the coastal to the open ocean, that is, the net offshore transport, is increased by 0.02 Pg C year^{-1} (Figure S5) due to increased nutrient inputs.

3.5 | Consequences for changes in FCO$_2$

The rise in atmospheric CO$_2$ levels, reflected in *CO$_2$-induced* perturbations (Figures 9g,j and 10d), is by far the dominant driver of changes in FCO$_2$ at the global scale, causing an increased uptake of 1.69 Pg C year^{-1} from the atmosphere over the 1905–2010 period. The open ocean is the major contributor to this increased sink owing to the ocean carbon dissolution pump, with an uptake of 1.63 Pg C year^{-1} (Figure 10d). The uptake of the coastal ocean in this scenario contributes only 0.06 Pg C year^{-1}. This corresponds to only around 4% of the global uptake of anthropogenic CO$_2$ by the global ocean.

The *climate-induced* perturbation of the ocean leads to a decrease in the total oceanic uptake of atmospheric CO$_2$ by about 0.1 Pg C year^{-1} over the simulation period (Figures 9g,i and 10d). While the changes caused by the perturbation of the hydrodynamical features are spatially very heterogeneous, the global simulated outgassing signal is mostly driven by the open ocean at northern tropical and subtropical latitudes, as well as in the southern midlatitudes (Figures 10e and 12b), in regions where the model also simulates a strong increase in SST (Figure 7a). Despite the global mean increase in coastal ocean temperature, the model does not simulate a statistically significant change in the global coastal FCO$_2$ as a result of the changing physical climate.

In contrast, *terr. nut-induced* perturbations lead to a marginal increase in the global oceanic CO$_2$ uptake (+0.03 Pg C year^{-1}), with the model simulating an increase in uptake of atmospheric CO$_2$ by the coastal ocean of 0.02 Pg C year^{-1} as a result of these perturbations (Figures 10d and 12c).

Taking into account all perturbations, the oceanic CO$_2$ uptake approximately increases by 1.77 Pg C year^{-1} between 1905 and 2010 (Figure 10d), with total increases of 1.66 and 0.09 Pg C year^{-1} for the open and coastal oceans, respectively. The increases in the CO$_2$ uptake flux density in the coastal and open ocean are thereby 3.6 and 5.4 g C m^{-2} year^{-1} for global areas of approximately 25×10^6 km^2 and 336×10^6 km^2, respectively. In the coastal ocean, generally, an uptake of atmospheric CO$_2$ of over 8 g C m^{-2} year^{-1} is simulated regionally due to all perturbations, especially in mid-to-high latitudes. Many tropical regions, such as the Sunda and west tropical Atlantic
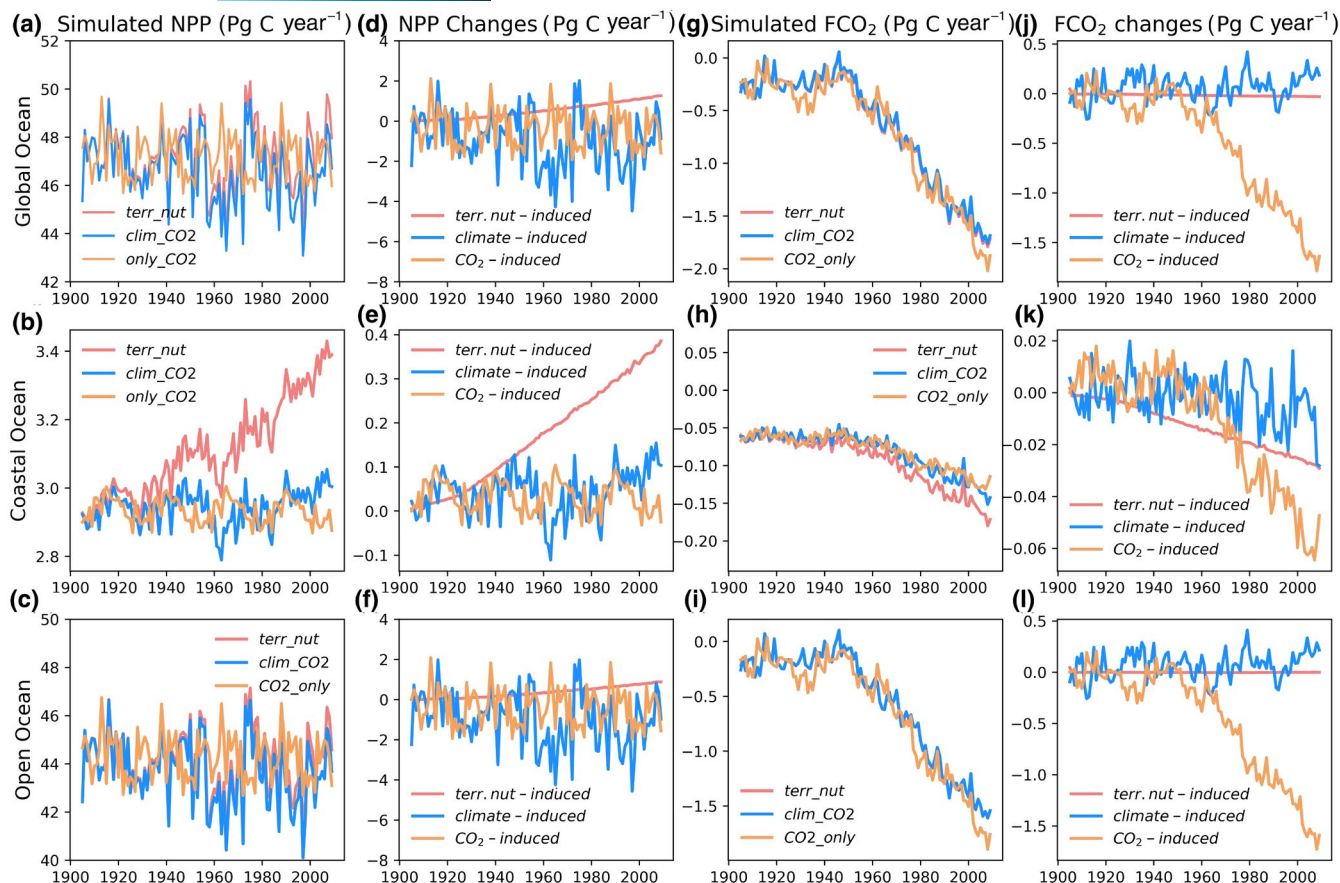
FIGURE 9 Temporal evolution of global annual mean NPP (two left columns) and FCO_2 (two right columns) over the 1905–2010 period for the global ocean (top row), coastal ocean (middle row) and open ocean (bottom row) in the simulations *only_CO2*, *clim_CO2* and *terr_nut* (panels a–c and g–i). Panels (d–f) and (j–l) illustrate changes in NPP (two left columns) and FCO_2 (two right columns) as a result of increases in atmospheric CO_2 levels (*CO2-induced*), perturbations in the physical climate (*climate-induced*) and increased terrigenous P and N inputs to the ocean (*terr. nut-induced*)perturbations. A positive FCO_2 corresponds to a flux from the ocean to the atmosphere

shelves, however, are simulated as areas with much lower increases in net CO_2 uptake flux density than the global ocean average, and large parts of the Arctic do not show a statistically significant change with respect to the change in FCO_2 (Figure 12d).

3.6 | Regional-scale changes for coastal NPP and FCO_2

Changes in both NPP and FCO_2 arising from CO_2-, *climate-* and *terr. nut-induced* perturbations differ strongly from one coastal region to the next over the simulated 1905–2010 time period (Figures 11 and 12). At the large scale, the most important *terr. nut-induced* changes in NPP are simulated for tropical Indian ocean shelves (Figure 13a,b). Here, riverine P and N inputs increase by 0.2 Tg P year^{-1} and 3.6 Tg N year^{-1}, respectively, causing a regional NPP increase of 38 g C m^{-2} year^{-1}, or 37% in relative terms. In general, northern mid-latitude shelves undergo the largest changes, thus reflecting the distribution of riverine perturbations (Figure 4). Indeed, rivers supplying nutrients in these regions undergo increases of 0.53 Tg P year^{-1} (+31%) and 5.2 Tg N year^{-1} (+78%), causing increases in the northern

mid-latitude Pacific and Atlantic shelves NPP of 36 g C m^{-2} year^{-1} (+24%) and 23 g C m^{-2} year^{-1} (+17%), respectively. Despite these large *terr. nut-induced* increases in NPP at the regional large scale, these perturbations do not substantially affect the large-scale regional FCO_2 (Figure 13c,d) in comparison to *atm. CO_2*- and *climate-induced* changes. While CO_2-*induced* perturbations have a consistent negative effect on the sign of the FCO_2, meaning increased uptake or decreased outgassing, for all segments of the coastal ocean analysed here (Figure 13c), *climate-induced* perturbations lead to both positive and negative changes in FCO_2, depending on the region (Figure 13d).

At the finer regional scale, the impacts of different perturbations on regionalized NPP and FCO_2 vary even more (Figure 14a–l). While the trends in NPP caused by *climate-induced* changes over the whole simulation period are weak for our chosen regions, strong inter-annual to decadal variability are simulated, for instance during years 1970–1980 on the eastern North American shelf, as well as after year 2000 for the Sunda shelf and southern North Sea (Figure 14a,c,d). Increased terrigenous nutrient inputs increase the NPP in all selected regions and clearly dominate the NPP trend throughout the simulation period, although the relative changes vary strongly from one region to another. For instance, while the annual mean

FIGURE 10 Mean annual changes in (a) NPP and (d) FCO$_2$ over the 1905–2010 period for the global, coastal and open ocean. Panels (b) and (e) show *climate-induced* perturbations for different latitudinal bands and (c) and (f) show *terr. nut-induced* changes for different ocean basins. Dashed lines indicate a statistically significant trend at $p < 0.05$. A positive FCO$_2$ corresponds to a flux from the ocean to the atmosphere
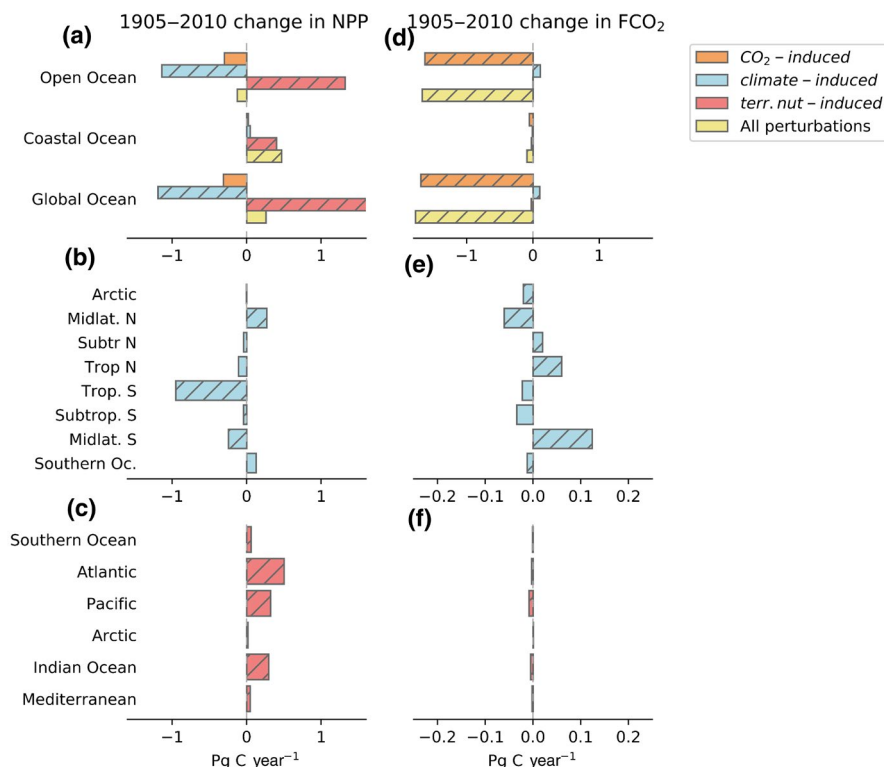
NPP increases by only around 12% in the eastern North American shelf, the perturbation is more substantial in the East China Sea, the southern North Sea, the Louisiana shelf and on the shelves of the Bay of Bengal, with relative increases of 42%, 41%, 97% and 162% simulated in these regions, respectively (Figure 14b,d,e,f). For the Louisiana shelf and the Bay of Bengal shelves, riverine P and N inputs rose more than threefold and fivefold, respectively. While simulated *CO$_2$-induced* perturbations are responsible for the largest impacts on the FCO$_2$ trend in the East China Sea and Eastern North American shelf for 1905–2010, *terr. nut-induced* perturbations are the most important contributors to the change in FCO$_2$ on the Sunda shelf, in the southern North Sea, on the Louisiana shelf and on shelves of the Bay of Bengal. Indeed, dramatic increases in the regional FCO$_2$ of over 10 g C m^{-2} year^{-1} are simulated in the latter two regions. We note that these strong changes in FCO$_2$ for these riverine-dominated shelves are, however, not representative of the behaviour of the coastal ocean as a whole (Figure 12c).
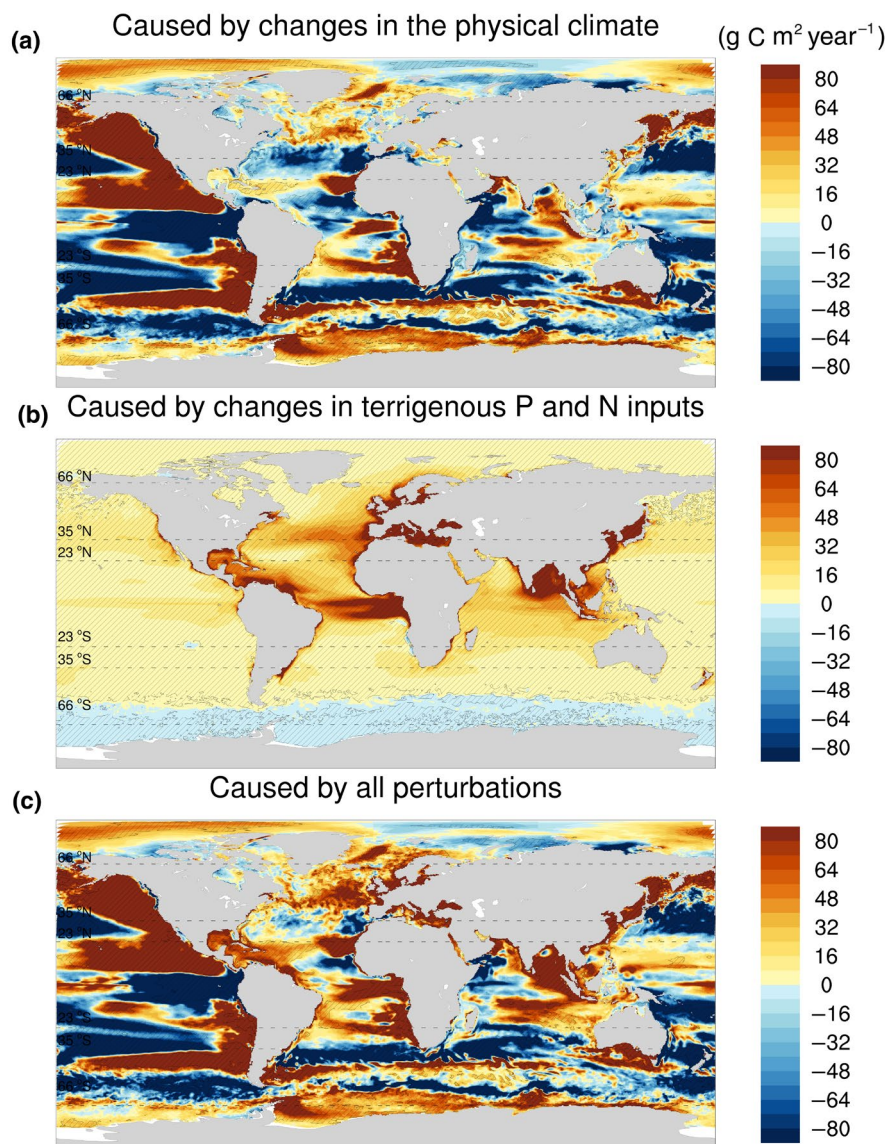
4 | DISCUSSION

4.1 | Role of changes in the physical climate for oceanic carbon cycling

The increased storage of heat in the ocean caused an increase in near-surface seawater temperatures over the historical time period (Rhein et al., 2013), which should, in theory, increase the stratification of the upper ocean. Increased stratification, in turn, decreases vertical mixing in near surface ocean waters, thus inhibiting the supply of

nutrients from intermediate depths to the euphotic zone. The NPP should thus also decrease as a result (Behrenfeld et al., 2006). Our model results confirm this hypothesis to a certain degree, since they first show widespread increases in ocean surface temperatures as a result of changes in the air–sea heat flux balance. This leads to a globally integrated decrease in the mean MLD, thus signalling increased stratification. Our simulations suggest that the strongly heterogeneous spatial patterns in MLD changes are dictated by local changes in circulation, which are themselves driven by either changes in atmospheric circulation, in physical features within the ocean (e.g. density) or a combination of these. Indeed, both changes in atmospheric circulation and in physical oceanic features have been reported to be disturbed at coarse and fine scales (Church et al., 2011; Kuhlbrodt & Gregory, 2012; Pershing et al., 2018; Rhein et al., 2013). As a result, the same geographical locations in the ocean may progressively be supplied with waters of different physical characteristics, explaining why local SST trends are not always reflected in the MLD trends (Figure 7a,b). Despite this complex spatial evolution of the simulated MLD, over the global scale, we simulate a decline of the oceanic NPP of about 3%, likely owing to the inhibition of vertical mixing and of nutrient supply at the large-scale during winter. Here again, however, local changes in NPP are also strongly variable, with both areas of substantial increases and decreases simulated in the model. Our simulations thus suggest that changes in ocean circulation might have a much larger regional importance on the NPP than the sole effect of large-scale stratification from the perturbation of the air–sea heat exchange at the local scale.

Local changes in ocean circulation seem to be of even larger importance in the coastal ocean, where hydrodynamical circulation

1905–2010 changes in NPP

(a) Caused by changes in the physical climate   (g C m² year⁻¹)

(b) Caused by changes in terrigenous P and N inputs


(c) Caused by all perturbations

FIGURE 11 1905–2010 changes in the annual mean NPP arising from (a) perturbations in the physical climate (*climate-induced*), (b) increased terrigenous P and N inputs to the ocean (*terr. nut-induced*) and (c) both perturbations combined. Dashed areas represent areas with significant trend ($p < 0.05$)

changes along the shelf break play a major role in the spatial variability of the SST and MLD, since the open ocean supplies waters with very different physical characteristics to the coastal ocean. For instance, the perturbation of the exchange with open waters at the shelf break has already been demonstrated at the regional scale (Gulf of Maine: Pershing et al., 2018; Outer North Sea shelf: Mathis et al., 2019). The very different magnitudes of change in our simulations show the difficulty to assess at the global scale due to the heterogeneity and complexity of coastal ocean circulation features.

While decadal variability of the ocean system currently prevents definite conclusions regarding the impacts of climate-induced changes on the biological productivity from observations alone, modelling studies have addressed these perturbations at global (Bopp et al., 2013; Laufkötter et al., 2013, 2015; Matsumoto et al., 2010) and regional scales (Fennel et al., 2006; Frischknecht et al., 2018; Holt et al., 2016, 2018; Mathis et al., 2019). In Laufkötter et al. (2013), the trend in the aggregated global NPP was quantified over the second

half of the 20th century, yielding a decrease in both the global NPP and biological export production in the magnitude of 6%, whereas in Matsumoto et al. (2010), no substantial change in the biological export production was found. The differences between these results, and those presented here, which suggest a climate-induced NPP decrease of around 3%, may be a consequence of the use of different modelling frameworks in each study. First, our horizontal spatial resolution is around fourfold higher than in most previous global modelling studies on historical changes in oceanic NPP, allowing a finer-scale representation of hydrodynamics in the ocean. The higher resolution of our model therefore likely simulates the regional response of the ocean circulation to changes in atmospheric drivers more accurately. Second, however, Laufkötter et al. (2013) and Matsumoto et al. (2010) used a fully coupled Earth System Model that accounts for feedbacks between atmospheric and oceanic processes while our modelling framework relies on a prescribed atmospheric state. Third, the global response of hydrodynamical and biogeochemical processes

1905–2010 changes in FCO$_2$
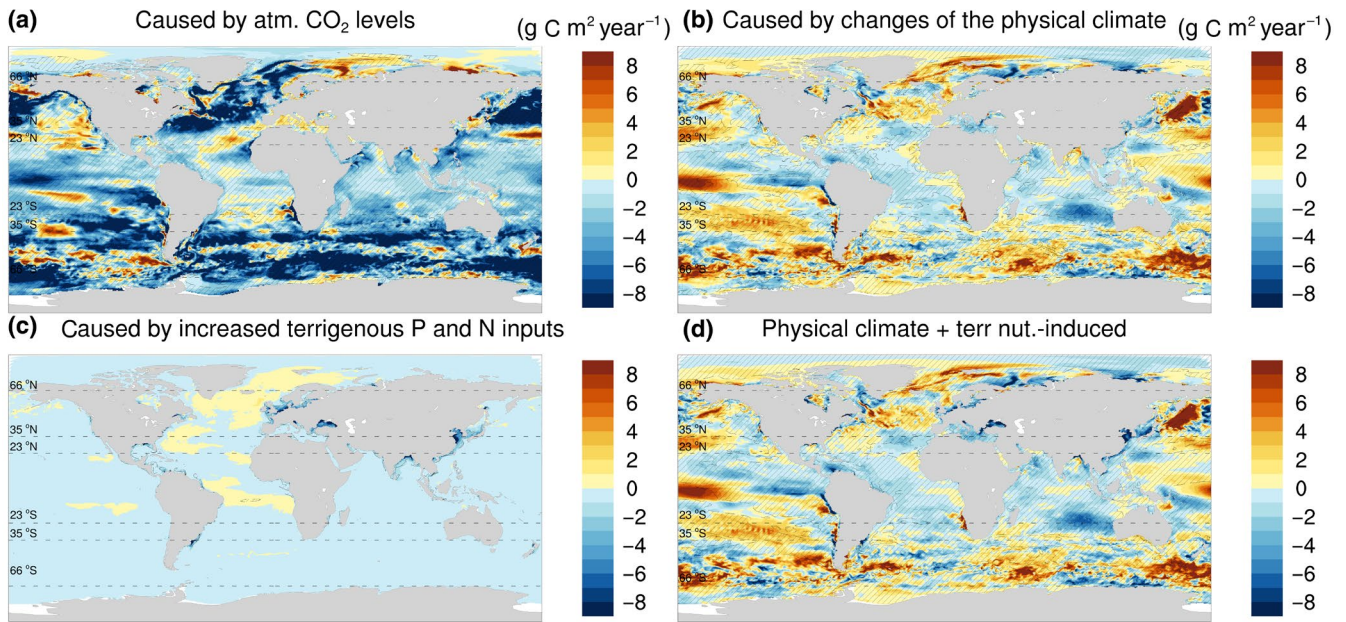
FIGURE 12 1905–2010 changes in the annual mean FCO$_2$ arising from (a) increases in atmospheric CO$_2$ levels (*CO$_2$-induced*), (b) changes in physical climate (*climate-induced*), (c) increased terrigenous nutrient inputs (*terr. nut-induced*) and (d) changes in the physical climate and increased terrigenous nutrient inputs combined (*climate-induced+terr. nut-induced*). A positive FCO$_2$ indicates a flux from the ocean to the atmosphere. Dashed areas represent areas with statistical significance at $p < 0.05$
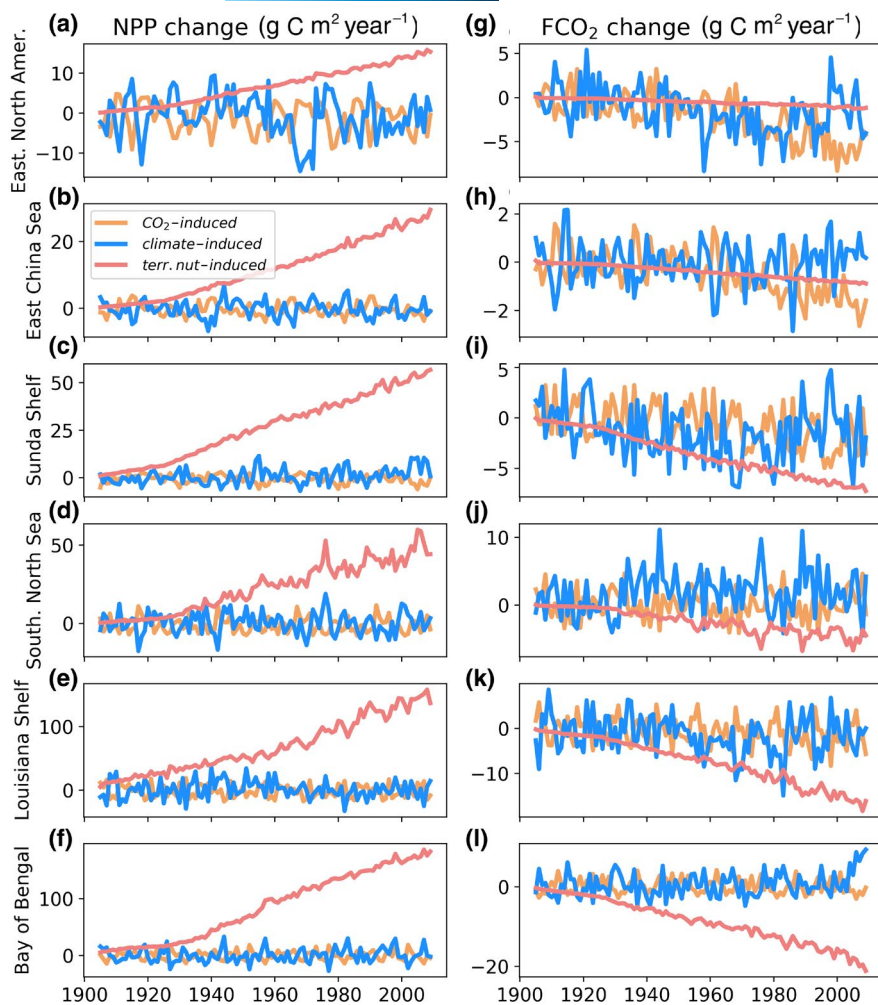
FIGURE 13 Large-scale regionalized changes in annual NPP and FCO$_2$ caused by *CO$_2$-*, *climate-* and *terr. nut-induced* perturbations over the 1905–2010 period. Panels (a) and (b) show the impacts of *terr. nut-induced* perturbations (*x*-axis) against *climate-induced* (*y*-axis) perturbations in absolute and relative terms, respectively. Panels (c) and (d) show the impacts of *terr. nut-induced* perturbations (*x*-axis) against *CO$_2$-induced* (*y*-axis) and *climate-induced* (*y*-axis) perturbations, respectively. A positive FCO$_2$ flux indicates a flux from ocean to atmosphere
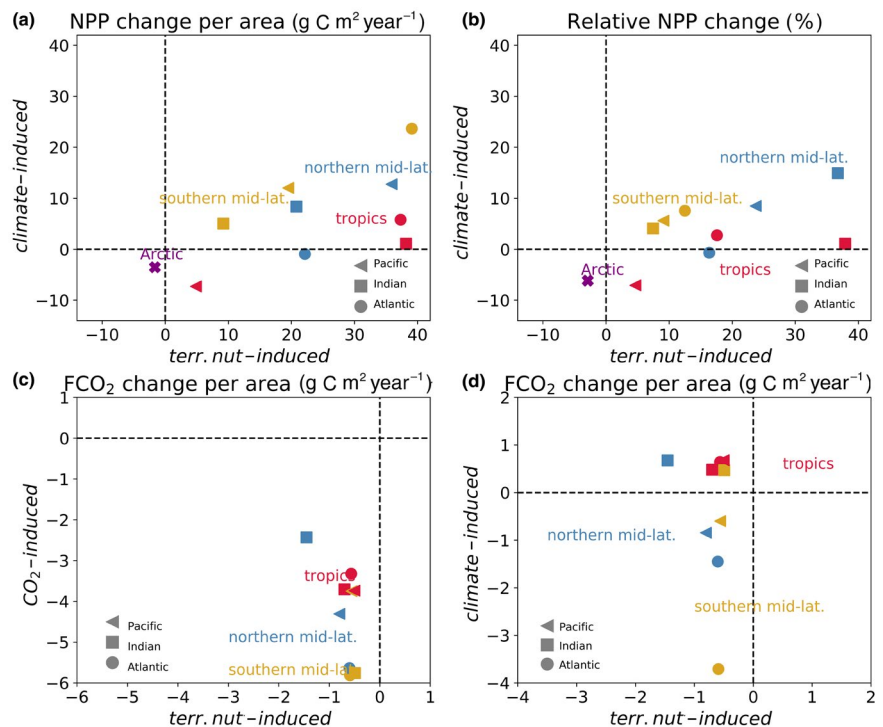
to changes in the physical climate has been shown to strongly vary from one model to the other (Bopp et al., 2013; Kwiatkowski et al., 2017, 2020; Laufkötter et al., 2015; Mathis & Mikolajewicz, 2020; Matsumoto et al., 2010). Thus, the trend in the marine NPP is also strongly affected by the different architectures and formulations for hydrodynamical and biogeochemical processes in different models.

4.2 | Role of increased terrigenous nutrient inputs for oceanic carbon cycling

Regional observation-based and model-based studies have reported both strong alterations of coastal biogeochemical indicators caused by increases in riverine P and N inputs. These perturbations include

FIGURE 14 Regionalized changes in annual NPP (panels a–f) and FCO_2 over the 1905–2005 period as a result of *CO_2-induced* and *climate-induced* and *terr-nut-induced* perturbations. A positive FCO_2 indicates a flux from ocean to atmosphere

changes in nutrient regimes, increased biological productivity and decreasing oxygen concentrations in the coastal ocean (Breitburg et al., 2018; Diaz & Rosenberg, 2008; Fennel & Testa, 2019; Rabalais et al., 2002). Even substantial regional FCO_2 changes have been traced back to terrigenous nutrient supplies locally (Cotovicz et al., 2015; Tseng et al., 2011). In GOBMs, which are essential components of Earth system models that are used for climate change projections (e.g. Aumont et al., 2015; Bourgeois et al., 2016; Dunne et al., 2012, 2020; Mauritsen et al., 2019; Tjiputra et al., 2020), temporal changes in riverine nutrient fluxes and their impacts on and beyond the coastal ocean have, however, yet to be taken into account.

In our model simulations, we simulate a 5% increase in the global ocean NPP between 1905 and 2010 due to the augmented terrigenous nutrient supply to the ocean. This increase is slightly larger in magnitude than our simulated decline of the global NPP induced by the physical perturbation of the ocean and is comparable to the climate-induced decrease in NPP of around 6% reported by Laufkötter et al. (2013), although it should be noted that the Laufkötter et al. (2013) study accounts only for the second half of the 20th century. The coastal ocean is, unsurprisingly, strongly affected in relative terms, undergoing an NPP increase of 14% induced by increased land-derived nutrient inputs, confirming reported widespread increases in biological productivity and eutrophication in

coastal regions over the past century (Fennel & Testa, 2019). The increase is, thus, for the coastal ocean overall, considerably lower than the relative increase in riverine P and N supplies to the ocean (+43% and +70%, respectively), although this effect is certainly regionally dependent. It is also lower than increases in biological productivity of up to +50% reported in early conceptual box model assessments (Andersson et al., 2005; Mackenzie et al., 2004; Rabouille et al., 2001; Ver et al., 1999). As demonstrated in our analysis of individual regions (Figure 14), however, increases in terrigenous nutrient supplies to the ocean may have caused more than a twofold NPP increase regionally since 1905. This, in turn, might have contributed to adverse environmental impacts such as increased hypoxia (Fennel & Testa, 2019). Despite these potential dramatic consequences regionally, our results suggest that open ocean inflows have a very prominent role in supplying global coastal waters with nutrients, as suggested by ocean inflows versus freshwater contributions to the global coastal ocean in Lacroix et al. (2021). Inflows from the open ocean have been demonstrated to majorly dictate biogeochemical dynamics in a multitude of coastal regions (Outer North Sea: Mathis et al., 2019; Thomas et al., 2005, North America East Coast: Fennel and Wilkin, 2009, California Current System: Frischknecht et al., 2018; South China Sea: Dai et al., 2013) while others are clearly driven by riverine inputs (Amazon plume: Louchard et al., 2021,

Louisiana Shelf: Große et al., 2019, Sylvan et al., 2006), or for which the dominant controls are still debated (East China Sea: Große et al., 2020; Zhang et al., 2019).

The simulated nutrient input-induced increase of the NPP in the open ocean also suggests that perturbations of nutrient inputs to the coastal ocean, arising largely from rivers, impact biological productivity beyond the coastal ocean. This is caused, on the one hand, by an increase in the nutrient cross-shelf export from the coastal ocean to the open ocean ($+0.4$ Tg P year^{-1} and $+12$ Tg N year^{-1}) and, on the other hand, by increased N inputs to the open ocean resulting from direct atmospheric deposition (around 4 Tg N year^{-1}) over the 20th century. According to our model, the increased supply of N to the open ocean is, therefore, larger as a result of exports from the coastal zone rather than increased inputs from atmospheric deposition. The relative increase in the open ocean NPP of around 4% as a result of the increased land-to-ocean inputs, however, remains low due to the dilution effect of the vast open ocean basin. Our model realizations also show that some open ocean regions could be disproportionally impacted by perturbations in riverine nutrient transports, such as the Indian Ocean, the Tropical Atlantic and North Atlantic, as well as the Caribbean Sea (Figure 11).

Despite a considerable increase in biological productivity, the sensitivity of the global oceanic FCO_2 to the land-induced perturbation is low in the model because the ocean NEP is only marginally altered. This low sensitivity of the FCO_2 to the NPP increase stems from the inefficient transfer of biologically fixed carbon to the deeper layers of the ocean due to the fast remineralization of organic matter in the stratified open ocean. For parts of the shallow coastal ocean, however, the increase in the uptake of atmospheric CO_2 induced by increased riverine P and N inputs is significant, due to the faster removal of the newly produced organic matter through either horizontal (i.e. offshore export) or vertical transport (i.e. deposition and burial on the seafloor). This is in particular the case for the East China Sea, the southern North Sea, the Louisiana shelf, as well as on Bay of Bengal shelves, where nutrient increases appear to be the largest contributor to changes in the regionalized FCO_2. This importance of nutrient inputs for changes in regional CO_2 uptake corroborates with observation-based findings for a tropical and a subtropical coastal system (Brazilian shelf: Cotovicz et al., 2015; East China Sea: Tseng et al., 2011).

4.3 | Implications for the anthropogenic CO_2 uptake of the coastal ocean

The role of the coastal ocean in taking up anthropogenic CO_2 has been strongly debated over the past three decades (Andersson et al., 2005; Bauer et al., 2013; Bourgeois et al., 2016; Cai, 2011; Chen and Borges, 2009; Laruelle et al., 2014, 2018; Mackenzie et al., 1998; Rabouille et al., 2001). While conceptual box models have suggested that the coastal ocean is a stronger atmospheric sink of anthropogenic CO_2 than the open ocean (Andersson et al., 2005; Mackenzie et al., 2004; Rabouille et al., 2001), model results from the only globally spatially resolved study on the anthropogenic perturbation of the coastal FCO_2 published to date (Bourgeois et al., 2016) suggest that coastal ocean is an inefficient sink of

anthropogenic carbon. Temporal changes in riverine nutrient inputs were, however, not considered in the simulations of Bourgeois et al. (2016), a factor considered to be significant for the global coastal FCO_2 uptake in the conceptual box model studies. Our model, in turn, indicates that the effects of enhanced terrigenous nutrient inputs on the coastal FCO_2, at the global scale, might be smaller than previously thought. A likely explanation for this is the strong overestimation of CWRT in the conceptual box model studies, as shown in Lacroix et al. (2021), which certainly cause a slower export of increased nutrients offshore than in our study, thus increasing their exposure time in the coastal ocean (Monsen et al., 2002).

In addition to this, results from the observation-based study of Laruelle et al. (2018) imply that the coastal ocean could be more efficient at taking up anthropogenic CO_2 per unit surface area than the open ocean. Our model, in turn, simulates a smaller global increase in the coastal CO_2 flux density than in the open ocean. These differences may be explained by the spatial coverage of observational data in the Laruelle et al. (2018) study, which to a large degree, relies on data from mid-to-high latitudinal shelves, for which we find intense sinks of anthropogenic CO_2 in our model results (e.g. Eastern Coast of North America, Barents Sea, East China Sea). In addition to this, our model indicates that the CO_2 flux in several mid-to-high latitude regions may have additionally been substantially enhanced as a consequence of increased nutrient inputs of terrigenous origin and their enhancement of biological productivity (Figure 14, e.g. in the southern North Sea). In contrast, for large tropical regions and parts of the Arctic Ocean, our model indicates that the coastal ocean might be an inefficient sink of anthropogenic CO_2 per area. These regions have, until now, been sampled very sparsely and are thus underrepresented in the observational time-series of Laruelle et al. (2018).

Our model, while providing global coverage and a broad representation of coastal circulation features, is still very coarse with respect to the spatial scale of many processes taking place in the coastal ocean (Liu et al., 2019; Pätsch et al., 2017). For instance, biogeochemical transport via eddies, fine-scale currents, including currents at the shelf-break, and fronts are likely not adequately captured at our model's resolution, in contrast to regional models (e.g. Frischknecht et al., 2018; Gomez et al., 2020; Gruber et al., 2011; Hauri et al., 2020). These limitations likely affect the degree to which increased terrigenous nutrients impact the biological productivity of the coastal ocean, as well as the amount of nutrients exported offshore and how they may stimulate the biological productivity in the open ocean.

4.4 | Limitations induced by scenarios of riverine and atmospheric inputs

In addition to the model limitations in representing the fine-scale features of the coastal ocean discussed above and in Lacroix et al. (2021), the magnitudes of riverine P and N inputs to the ocean and their temporal changes are still associated with large uncertainties. This is reflected in the large spread of global estimates derived from upscaling of a relatively small number of catchments to the global scale (e.g. Compton et al., 2000; Meybeck, 1982). Global catchment-scale models (Beusen et al., 2016; Green et al., 2004; Seitzinger et al.,

2010; Van Drecht et al., 2005) have also proved difficult to calibrate and validate due to the strong hydrological and biogeochemical heterogeneity across temporal (i.e. seasonality, inter-annual variability) and spatial (e.g. basin characteristics) scales. As a result, the magnitudes of contemporary P and N fluxes to the ocean are substantially different in, for instance, the global modelling studies of Seitzinger et al. (2010) and Beusen et al. (2016), although the anthropogenic perturbations estimated in these studies are similar. The temporal changes in riverine P and N inputs are resolved in a simplified manner in our study, using first-order approximation between the start and end of the 20th century and thus, our results might deviate due to the assumed linear increases for individual river basins. For instance, in the Baltic Sea, riverine nutrient inputs are reported to have first increased from beginning to the middle of the 20th century, but to have decreased since the 1980s, which may have led to a stabilization of NPP trends in the region (Meier et al., 2019). In addition to this, we also do not account for the seasonality of the riverine nutrient inputs.

Inputs of other terrestrial-derived species, such as carbon and silica, have also been significantly perturbed by human activities (Maavara et al., 2017; Regnier et al., 2013) over the same period. While there is an overall consensus on an increase of the inputs of these elements to freshwater systems during the 20th century, the global retention of land-derived material has also increased along the land–ocean continuum, potentially counteracting increasing inputs to freshwater systems (Goll et al., 2014; Laruelle et al., 2009; Lauerwald et al., 2020; Maavara et al., 2014, 2017; Regnier et al., 2013). In this study, we focussed on changes to P and N inputs to the ocean that have arguably been the most perturbed by anthropogenic activities and thus omitted potential additional effects caused by alterations of other terrestrial-derived compounds.

We also did not consider changes in atmospheric P deposition throughout the simulation period. This choice was guided by the relatively small pre-industrial background atmospheric deposition flux of biologically available P to the ocean (0.2 Tg P year^{-1}, Mahowald et al., 2008) compared to riverine P fluxes (2–11 Tg P year^{-1}, Beusen et al., 2016; Compton et al., 2000; Seitzinger et al., 2010), and by the small anthropogenic perturbation of this flux, estimated in the order of 10% (Mahowald et al., 2008).

5 | CONCLUSIONS

Large uncertainties are still withstanding regarding processes that control the oceanic carbon fluxes and their anthropogenic perturbations. In this study, we assessed, for the first time, the implications of increased terrigenous inputs of the nutrients P and N for the oceanic carbon cycle over the past century in a global ocean biogeochemical model, and contrasted these changes to those induced by increasing atmospheric CO_2 levels and a changing physical climate. Our results, which cover the 1905–2010 period, indicate that the perturbation induced by terrigenous nutrients causes a notable increase in the global ocean NPP that could be of similar magnitude to the highly uncertain NPP

decline arising from changes in the physical climate. Thus, they may alleviate the certain effects induced by physical climate changes on the ocean carbon cycle. Our results are especially relevant for the biological productivity of the global coastal ocean, and in particular in northern mid-latitudes and low latitudes, where changes in NPP are dominated by the enhanced riverine fluxes of nutrients over the simulation timespan. These changes in organic matter production could be important triggers of coastal hypoxia, which have been reported to have dramatic effects for coastal ecosystems and marine life (Fennel & Testa, 2019). In the coastal ocean, the increase in P and N inputs also increases the air–sea CO_2 uptake via enhancement of the biological carbon pump. These increased P and N inputs are the major drivers of change in the FCO_2 in certain river-dominated regions (southern North Sea, Louisiana shelf, Bay of Bengal shelves). Nevertheless, this globally enhanced coastal CO_2 uptake is smaller than what has been suggested using conceptual box models until now, confirming a weak efficiency of the coastal ocean in taking-up anthropogenic CO_2 reported in Bourgeois et al. (2016) and Lacroix et al. (2021). The increase in terrigenous nutrient inputs also has a further-reaching effect on the NPP of the ocean as a whole than previously assumed. In particular, increased riverine nutrients may be exported offshore relatively efficiently where they could potentially affect ecosystems in the open ocean. On the whole, our study indicates that, along with improvements in the representation of both biogeochemical and physical processes taking place in the coastal ocean, past and future temporal dynamics of riverine nutrient inputs should be included in global ocean biogeochemical models to better constrain oceanic carbon fluxes and their anthropogenic perturbations.

ORCID

Fabrice Lacroix https://orcid.org/0000-0003-4749-2826

REFERENCES

Andersson, A. J., Mackenzie, F., & Lerman, A. (2005). Coastal ocean and carbonate systems in the high CO_2 world of the Anthropocene. *American Journal of Science*, 305, 875–918. https://doi.org/10.2475/ajs.305.9.875

Aumont, O., Ethé, C., Tagliabue, A., Bopp, L., & Gehlen, M. (2015). PISCES-v2: An ocean biogeochemical model for carbon and ecosystem studies. *Geoscientific Model Development*, 8(8), 2465–2513. https://doi.org/10.5194/gmd-8-2465-2015

Bauer, J., Cai, W. J., Raymond, P., Bianchi, T. S., Hopkinson, C. S., & Regnier, P. A. G. (2013). The changing carbon cycle of the coastal ocean. *Nature*, 504, 61–70. https://doi.org/10.1038/nature12857

Beaulieu, C., Henson, S. A., Sarmiento, J. L., Dunne, J. P., Doney, S. C., Rykaczewski, R. R., & Bopp, L. (2013). Factors challenging our ability to detect long-term trends in ocean chlorophyll. *Biogeosciences*, 10(4), 2711–2724. https://doi.org/10.5194/bg-10-2711-2013

Beaulieu, E., Goddéris, Y., Donnadieu, Y., Labat, D., & Roelandt, C. (2012). High sensitivity of the continental-weathering carbon dioxide sink to future climate change. *Nature Climate Change*, 2(5), 346–349. https://doi.org/10.1038/nclimate1419

Behrenfeld, M. J., O'Malley, R. T., Siegel, D. A., McClain, C. R., Sarmiento, J. L., Feldman, G. C., Milligan, A. J., Falkowski, P. G., Letelier, R. M., & Boss, E. S. (2006). Climate-driven trends in contemporary ocean productivity. *Nature*, 444(7120), 752–755. https://doi.org/10.1038/nature05317

Beusen, A. H. W., Bouwman, A. F., Van Beek, L. P. H., Mogollón, J. M., & Middelburg, J. J. (2016). Global riverine N and P transport to ocean increased during the 20th century despite increased retention along the aquatic continuum. *Biogeosciences*, 13(8), 2441–2451. https://doi.org/10.5194/bg-13-2441-2016

Bopp, L., Resplandy, L., Orr, J. C., Doney, S. C., Dunne, J. P., Gehlen, M., Halloran, P., Heinze, C., Ilyina, T., Séférian, R., Tjiputra, J., & Vichi, M. (2013). Multiple stressors of ocean ecosystems in the 21st century: Projections with CMIP5 models. *Biogeosciences*, 10(10), 6225–6245. https://doi.org/10.5194/bg-10-6225-2013

Boucher, O., Servonnat, J., Albright, A. L., Aumont, O., Balkanski, Y., Bastrikov, V., Bekki, S., Bonnet, R., Bony, S., Bopp, L., Braconnot, P., Brockmann, P., Cadule, P., Caubel, A., Cheruy, F., Codron, F., Cozic, A., Cugnet, D., D'Andrea, F., … Vuichard, N. (2020). Presentation and evaluation of the IPSL-CM6A-LR climate model. *Journal of Advances in Modeling Earth Systems*, 12, e2019MS002010. https://doi.org/10.1029/2019MS002010

Bourgeois, T., Orr, J. C., Resplandy, L., Terhaar, J., Ethé, C., Gehlen, M., & Bopp, L. (2016). Coastal-ocean uptake of anthropogenic carbon. *Biogeosciences*, 13(14), 4167–4185. https://doi.org/10.5194/bg-13-4167-2016

Bouwman, A. F., Van Drecht, G., Knoop, J. M., Beusen, A. H. W., & Meinardi, C. R. (2005). Exploring changes in river nitrogen export to the world's oceans. *Global Biogeochemical Cycles*, 19(1). https://doi.org/10.1029/2004GB002314

Boyer, T. P., Garcia, H. E., Locarnini, R. A., Zweng, M. M., Mishonov, A. V., Reagan, J. R., Weathers, K. A., Baranova, O. K., Seidov, D., & Smolyar, I. V. (2018). World Ocean Atlas 2018. NOAA National Centers for Environmental Information. Dataset. https://accession.nodc.noaa.gov/NCEI-WOA18

Breitburg, D., Levin, L. A., Oschlies, A., Grégoire, M., Chavez, F. P., Conley, D. J., Garçon, V., Gilbert, D., Gutiérrez, D., Isensee, K., Jacinto, G. S., Limburg, K. E., Montes, I., Naqvi, S. W. A., Pitcher, G. C., Rabalais, N. N., Roman, M. R., Rose, K. A., Seibel, B. A., … Zhang, J. (2018). Declining oxygen in the global ocean and coastal waters. *Science*, 359(6371), eaam7240. https://doi.org/10.1126/science.aam7240

Cai, W.-J. (2011). Estuarine and coastal ocean carbon paradox: CO_2 sinks or sites of terrestrial carbon incineration? *Annual Review of Marine Science*, 3(1), 123–145. https://doi.org/10.1146/annurev-marine-120709-142723

Carr, M.-E., Friedrichs, M. A. M., Schmeltz, M., Noguchi Aita, M., Antoine, D., Arrigo, K. R., Asanuma, I., Aumont, O., Barber, R., Behrenfeld, M., Bidigare, R., Buitenhuis, E. T., Campbell, J., Ciotti, A., Dierssen, H., Dowell, M., Dunne, J., Esaias, W., Gentili, B., … Yamanaka, Y. (2006). A comparison of global estimates of marine primary production from ocean color. *Deep Sea Research Part II: Topical Studies in Oceanography*, 53(5), 741–770. https://doi.org/10.1016/j.dsr2.2006.01.028

Chen, C.-T.-A., & Borges, A. (2009). Reconciling opposing views on carbon cycling in the coastal ocean: Continental shelves as sinks and near-shore ecosystems as sources of atmospheric CO_2. *Deep Sea Research Part II: Topical Studies in Oceanography*, 56(8-10), 578–590. https://doi.org/10.1016/j.dsr2.2009.01.001

Church, J. A., White, N. J., Konikow, L. F., Domingues, C. M., Cogley, J. G., Rignot, E., Gregory, J. M., van den Broeke, M. R., Monaghan, A. J., & Velicogna, I. (2011). Revisiting the Earth's sea-level and energy budgets from 1961 to 2008. *Geophysical Research Letters*, 38(18). https://doi.org/10.1029/2011GL048794

Compton, J., Mallinson, D., Glenn, C., Filippelli, G., Föllmi, K., Shields-Zhou, G., & Zanin, Y. (2000). Variations in the global phosphorus cycle. In C. Glenn, L. Prévôt-Lucas, & J. Lucas (Eds.), *Marine authigenesis: From global to microbial* (Vol. 66, pp. 21–33). SEPM Special Publications.

Cotovicz, Jr., L., Knoppers, B., Brandini, N., Santos, S., & Abril, G. (2015). A strong CO_2 sink enhanced by eutrophication in a tropical coastal embayment (Guanabara Bay, Rio de Janeiro, Brazil). *Biogeosciences*, 12, 6125–6146. https://doi.org/10.5194/bg-12-6125-2015

Dai, M., Cao, Z., Guo, X., Zhai, W., Liu, Z., Yin, Z., Xu, Y., Gan, J., Hu, J., & Du, C. (2013). Why are some marginal seas sources of atmospheric CO_2? *Geophysical Research Letters*, 40(10), 2154–2158. https://doi.org/10.1002/grl.50390

Das, S., Giri, S., Das, I., Chanda, A., Ghosh, A., Mukhopadhyay, A., Akhand, A., Choudhury, S., Dadhwal, V., Maity, S., Kumar, T., Lotliker, A., Mitra, D., & Hazra, S. (2017). Nutrient dynamics of northern Bay of Bengal (nBoB)—Emphasizing the role of tides. *Regional Studies in Marine Science*, 10, 116–134. https://doi.org/10.1016/j.rsma.2017.01.006

Diaz, R. J., & Rosenberg, R. (2008). Spreading dead zones and consequences for marine ecosystems. *Science*, 321(5891), 926–929. https://doi.org/10.1126/science.1156401

Doney, S. C., Mahowald, N., Lima, I., Feely, R. A., Mackenzie, F. T., Lamarque, J.-F., & Rasch, P. J. (2007). Impact of anthropogenic atmospheric nitrogen and sulfur deposition on ocean acidification and the inorganic carbon system. *Proceedings of the National Academy of Sciences of the United States of America*, 104(37), 14580–14585. https://doi.org/10.1073/pnas.0702218104

Dunne, J. P., Horowitz, L. W., Adcroft, A. J., Ginoux, P., Held, I. M., John, J. G., Krasting, J. P., Malyshev, S., Naik, V., Paulot, F., Shevliakova, E., Stock, C. A., Zadeh, N., Balaji, V., Blanton, C., Dunne, K. A., Dupuis, C., Durachta, J., Dussin, R., … Zhao, M. (2020). The GFDL earth system model version 4.1 (GFDL-ESM 4.1): Overall coupled model description and simulation characteristics. *Journal of Advances in Modeling Earth Systems*, 12(11), e2019MS002015. https://doi.org/10.1029/2019MS002015

Dunne, J. P., John, J. G., Adcroft, A. J., Griffies, S. M., Hallberg, R. W., Shevliakova, E., Stouffer, R. J., Cooke, W., Dunne, K. A., Harrison, M. J., Krasting, J. P., Malyshev, S. L., Milly, P. C. D., Phillipps, P. J., Sentman, L. T., Samuels, B. L., Spelman, M. J., Winton, M., Wittenberg, A. T., & Zadeh, N. (2012). GFDL's ESM2 global coupled climate-carbon earth system models. Part I: Physical formulation and baseline simulation characteristics. *Journal of Climate*, 25(19), 6646–6665. https://doi.org/10.1175/JCLI-D-11-00560.1

Etheridge, D. M., Steele, L. P., Langenfelds, R. L., Francey, R. J., Barnola, J.-M., & Morgan, V. I. (1996). Natural and anthropogenic changes in atmospheric CO_2 over the last 1000 years from air in Antarctic ice and firn. *Journal of Geophysical Research: Atmospheres, 101*(D2), 4115–4128. https://doi.org/10.1029/95JD03410

Falkowski, P. G., Barber, R. T., & Smetacek, V. (1998). Biogeochemical controls and feedbacks on ocean primary production. *Science, 281*(5374), 200–206. https://doi.org/10.1126/science.281.5374.200

Fennel, K., & Testa, J. M. (2019). Biogeochemical controls on coastal hypoxia. *Annual Review of Marine Science, 11*(1), 105–130. https://doi.org/10.1146/annurev-marine-010318-095138

Fennel, K., & Wilkin, J. (2009). Quantifying biological carbon export for the northwest North Atlantic continental shelves. *Geophysical Research Letters, 36*, L18605. https://doi.org/10.1029/2009GL039818

Fennel, K., Wilkin, J., Levin, J., Moisan, J., O'Reilly, J., & Haidvogel, D. (2006). Nitrogen cycling in the Middle Atlantic Bight: Results from a three-dimensional model and implications for the North Atlantic nitrogen budget. *Global Biogeochemical Cycles, 20*(3). https://doi.org/10.1029/2005GB002456

Field, C. B., Behrenfeld, M. J., Randerson, J. T., & Falkowski, P. (1998). Primary production of the biosphere: Integrating terrestrial and oceanic components. *Science, 281*(5374), 237–240. https://doi.org/10.1126/science.281.5374.237

Friedlingstein, P., Jones, M. W., O'Sullivan, M., Andrew, R. M., Hauck, J., Peters, G. P., Peters, W., Pongratz, J., Sitch, S., Le Quéré, C., Bakker, D. C. E., Canadell, J. G., Ciais, P., Jackson, R. B., Anthoni, P., Barbero, L., Bastos, A., Bastrikov, V., Becker, M., … Zaehle, S. (2019). Global carbon budget 2019. *Earth System Science Data, 11*(4), 1783–1838. https://doi.org/10.5194/essd-11-1783-2019

Frischknecht, M., Münnich, M., & Gruber, N. (2018). Origin, transformation, and fate: The three-dimensional biological pump in the California current system. *Journal of Geophysical Research: Oceans, 123*(11), 7939–7962. https://doi.org/10.1029/2018JC013934

Galloway, J. N. (1995). Acid deposition: Perspectives in time and space. *Water, Air, and Soil Pollution, 85*(1), 15–24. https://doi.org/10.1007/BF00483685

Goll, D. S., Moosdorf, N., Hartmann, J., & Brovkin, V. (2014). Climate-driven changes in chemical weathering and associated phosphorus release since 1850: Implications for the land carbon balance. *Geophysical Research Letters, 41*, 3553–3558. https://doi.org/10.1002/2014GL059471

Gomez, F. A., Wanninkhof, R., Barbero, L., Lee, S.-K., & Hernandez, Jr., F. J. (2020). Seasonal patterns of surface inorganic carbon system variables in the Gulf of Mexico inferred from a regional high-resolution ocean biogeochemical model. *Biogeosciences, 17*(6), 1685–1700. https://doi.org/10.5194/bg-17-1685-2020

Green, P. A., Vörösmarty, C. J., Meybeck, M., Galloway, J. N., Peterson, B. J., & Boyer, E. W. (2004). Pre-industrial and contemporary fluxes of nitrogen through rivers: A global assessment based on typology. *Biogeochemistry, 68*(1), 71–105. https://doi.org/10.1023/B:BIOG.0000025742.82155.92

Große, F., Fennel, K., & Laurent, A. (2019). Quantifying the relative importance of riverine and open-ocean nitrogen sources for hypoxia formation in the Northern Gulf of Mexico. *Journal of Geophysical Research: Oceans, 124*(8), 5451–5467. https://doi.org/10.1029/2019JC015230

Große, F., Fennel, K., Zhang, H., & Laurent, A. (2020). Quantifying the contributions of riverine vs. oceanic nitrogen to hypoxia in the East China Sea. *Biogeosciences, 17*(10), 2701–2714. https://doi.org/10.5194/bg-17-2701-2020

Gruber, N., & Galloway, J. N. (2008). An Earth-system perspective of the global nitrogen cycle. *Nature, 451*, 293–296. https://doi.org/10.1038/nature06592

Gruber, N., Lachkar, Z., Frenzel, H., Marchesiello, P., Münnich, M., McWilliams, J. C., Nagai, T., & Plattner, G.-K. (2011). Eddy-induced reduction of biological production in eastern boundary upwelling systems. *Nature Geoscience, 4*, 787–792. https://doi.org/10.1038/ngeo1273

Harrison, J. A., Bouwman, A. F., Mayorga, E., & Seitzinger, S. (2010). Magnitudes and sources of dissolved inorganic phosphorus inputs to surface fresh waters and the coastal zone: A new global model. *Global Biogeochemical Cycles, 24*(1). https://doi.org/10.1029/2009GB003590

Hauri, C., Schultz, C., Hedstrom, K., Danielson, S., Irving, B., Doney, S. C., Dussin, R., Curchitser, E. N., Hill, D. F., & Stock, C. A. (2020). A regional hindcast model simulating ecosystem dynamics, inorganic carbon chemistry, and ocean acidification in the Gulf of Alaska. *Biogeosciences, 17*, 3837–3857. https://doi.org/10.5194/bg-17-3837-2020

Heinze, C., Maier-Reimer, E., Winguth, E. A., & Archer, D. (1999). A global oceanic sediment model for long-term climate studies. *Global Biogeochemical Cycles, 13*(1), 221–250. https://doi.org/10.1029/98GB02812

Henson, S. A., Sarmiento, J. L., Dunne, J. P., Bopp, L., Lima, I., Doney, S. C., John, J., & Beaulieu, C. (2010). Detection of anthropogenic climate change in satellite records of ocean chlorophyll and productivity. *Biogeosciences, 7*(2), 621–640. https://doi.org/10.5194/bg-7-621-2010

Holt, J., Polton, J., Huthnance, J., Wakelin, S., O'Dea, E., Harle, J., Yool, A., Artioli, Y., Blackford, J., Siddorn, J., & Inall, M. (2018). Climate-driven change in the north Atlantic and arctic oceans can greatly reduce the circulation of the north sea. *Geophysical Research Letters, 45*(21), 11811–11836. https://doi.org/10.1029/2018GL078878

Holt, J., Schrum, C., Cannaby, H., Daewel, U., Allen, I., Artioli, Y., Bopp, L., Butenschon, M., Fach, B. A., Harle, J., Pushpadas, D., Salihoglu, B., & Wakelin, S. (2016). Potential impacts of climate change on the primary production of regional seas: A comparative analysis of five European seas. *Progress in Oceanography, 140*, 91–115. https://doi.org/10.1016/j.pocean.2015.11.004

Ilyina, T., Six, K. D., Segschneider, J., Maier-Reimer, E., Li, H., & Núñez-Riboni, I. (2013). Global ocean biogeochemistry model HAMOCC: Model architecture and performance as component of the MPI-Earth system model in different CMIP5 experimental realizations. *Journal of Advances in Modeling Earth Systems, 5*(2), 287–315. https://doi.org/10.1029/2012MS000178

Jungclaus, J. H., Fischer, N., Haak, H., Lohmann, K., Marotzke, J., Matei, D., Mikolajewicz, U., Notz, D., & Storch, J. S. (2013). Characteristics of the ocean simulations in the Max Planck Institute Ocean Model (MPIOM) the ocean component of the MPI-Earth system model. *Journal of Advances in Modeling Earth Systems, 5*(2), 422–446. https://doi.org/10.1002/jame.20023

Kuhlbrodt, T., & Gregory, J. M. (2012). Ocean heat uptake and its consequences for the magnitude of sea level rise and climate change. *Geophysical Research Letters, 39*(18). https://doi.org/10.1029/2012GL052952

Kwiatkowski, L., Bopp, L., Aumont, O., Ciais, P., Cox, P. M., Laufkötter, C., Li, Y., & Séférian, R. (2017). Emergent constraints on projections of declining primary production in the tropical oceans. *Nature Climate Change, 7*(5), 355–358. https://doi.org/10.1038/nclimate3265

Kwiatkowski, L., Torres, O., Bopp, L., Aumont, O., Chamberlain, M., Christian, J. R., Dunne, J. P., Gehlen, M., Ilyina, T., John, J. G., Lenton, A., Li, H., Lovenduski, N. S., Orr, J. C., Palmieri, J., Santana-Falcón, Y., Schwinger, J., Séférian, R., Stock, C. A., … Ziehn, T. (2020). Twenty-first century ocean warming, acidification, deoxygenation, and upper-ocean nutrient and primary production decline from CMIP6 model projections. *Biogeosciences, 17*(13), 3439–3470. https://doi.org/10.5194/bg-17-3439-2020

Lacroix, F., Ilyina, T., & Hartmann, J. (2020). Oceanic CO_2 outgassing and biological production hotspots induced by pre-industrial river loads of nutrients and carbon in a global modeling approach. *Biogeosciences, 17*(1), 55–88. https://doi.org/10.5194/bg-17-55-2020

Lacroix, F., Ilyina, T., Laruelle, G. G., & Regnier, P. (2021). Reconstructing the pre-industrial coastal carbon cycle through a global ocean circulation model: Was the global continental shelf already both autotrophic and a CO_2 sink? *Global Biogeochemical Cycles*. https://doi.org/10.1029/2020GB006603

Landschützer, P., Gruber, N., & Bakker, D. C. E. (2016). Decadal variations and trends of the global ocean carbon sink. *Global Biogeochemical Cycles*, 30(10), 1396–1417. https://doi.org/10.1002/2015GB005359

Laruelle, G. G., Cai, W.-J., Hu, X., Gruber, N., Mackenzie, F. T., & Regnier, P. (2018). Continental shelves as a variable but increasing global sink for atmospheric carbon dioxide. *Nature Communications*, 9(1), 454. https://doi.org/10.1038/s41467-017-02738-z

Laruelle, G. G., Dürr, H. H., Lauerwald, R., Hartmann, J., Slomp, C. P., Goossens, N., & Regnier, P. A. G. (2013). Global multi-scale segmentation of continental and coastal waters from the watersheds to the continental margins. *Hydrology and Earth System Sciences*, 17(5), 2029–2051. https://doi.org/10.5194/hess-17-2029-2013

Laruelle, G. G., Landschützer, P., Gruber, N., Tison, J.-L., Delille, B., & Regnier, P. (2017). Global high-resolution monthly CO_2 climatology for the coastal ocean derived from neural network interpolation. *Biogeosciences*, 14(19), 4545–4561. https://doi.org/10.5194/bg-14-4545-2017

Laruelle, G. G., Lauerwald, R., Pfeil, B., & Regnier, P. (2014). Regionalized global budget of the CO_2 exchange at the air-water interface in continental shelf seas. *Global Biogeochemical Cycles*, 28, 1199–1214. https://doi.org/10.1002/2014GB004832

Laruelle, G. G., Roubeix, V., Sferratore, A., Brodherr, B., Ciuffa, D., Conley, D. J., Dürr, H. H., Garnier, J., Lancelot, C., Le Thi Phuong, Q., Meunier, J.-D., Meybeck, M., Michalopoulos, P., Moriceau, B., Ní Longphuirt, S., Loucaides, S., Papush, L., Presti, M., Ragueneau, O., … Van Cappellen, P. (2009). Anthropogenic perturbations of the silicon cycle at the global scale: Key role of the land-ocean transition. *Global Biogeochemical Cycles*, 23, GB4031. https://doi.org/10.1029/2008GB003267

Lauerwald, R., Regnier, P., Guenet, B., Friedlingstein, P., & Ciais, P. (2020). How simulations of the land carbon sink are biased by ignoring fluvial carbon transfers: A case study for the Amazon basin. *One Earth*, 3, 226–236. https://doi.org/10.1016/j.oneear.2020.07.009

Laufkötter, C., Vogt, M., & Gruber, N. (2013). Long-term trends in ocean plankton production and particle export between 1960–2006. *Biogeosciences*, 10(11), 7373–7393. https://doi.org/10.5194/bg-10-7373-2013

Laufkötter, C., Vogt, M., Gruber, N., Aita-Noguchi, M., Aumont, O., Bopp, L., Buitenhuis, E., Doney, S. C., Dunne, J., Hashioka, T., Hauck, J., Hirata, T., John, J., Le Quéré, C., Lima, I. D., Nakano, H., Seferian, R., Totterdell, I., Vichi, M., & Völker, C. (2015). Drivers and uncertainties of future global marine primary production in marine ecosystem models. *Biogeosciences*, 12(23), 6955–6984. https://doi.org/10.5194/bg-12-6955-2015

Laurent, A., Fennel, K., Cai, W.-J., Huang, W.-J., Barbero, L., & Wanninkhof, R. (2017). Eutrophication-induced acidification of coastal waters in the northern Gulf of Mexico: Insights into origin and processes from a coupled physical-biogeochemical model. *Geophysical Research Letters*, 44(2), 946–956. https://doi.org/10.1002/2016GL071881

Lee, M., Shevliakova, E., Stock, C. A., Malyshev, S., & Milly, P. C. D. (2019). Prominence of the tropics in the recent rise of global nitrogen pollution. *Nature Communications*, 10, 1437. https://doi.org/10.1038/s41467-019-09468-4

Le Fouest, V., Babin, M., & Tremblay, J.-É. (2013). The fate of riverine nutrients on Arctic shelves. *Biogeosciences*, 10(6), 3661–3677. https://doi.org/10.5194/bg-10-3661-2013

Levitus, S., Antonov, J., & Boyer, T. (2005). Warming of the world ocean, 1955–2003. *Geophysical Research Letters*, 32(2), 1955–2003. https://doi.org/10.1029/2004GL021592

Liljeström, I., Kummu, M., & Varis, O. (2012). Nutrient balance assessment in the Mekong basin: Nitrogen and phosphorus dynamics in a catchment scale. *International Journal of Water Resources Development*, 28(2), 373–391. https://doi.org/10.1080/07900627.2012.668649

Liu, X., Dunne, J. P., Stock, C. A., Harrison, M. J., Adcroft, A., & Resplandy, L. (2019). Simulating water residence time in the coastal ocean: A global perspective. *Geophysical Research Letters*, 46(23), 13910–13919. https://doi.org/10.1029/2019GL085097

Lønborg, C., & Álvarez-Salgado, X. A. (2012). Recycling versus export of bioavailable dissolved organic matter in the coastal ocean and efficiency of the continental shelf pump. *Global Biogeochemical Cycles*, 26(3). https://doi.org/10.1029/2012GB004353

Louchard, D., Gruber, N., & Münnich, M. (2021). The impact of the Amazon on the biological pump and the air-sea CO_2 balance of the Western Tropical Atlantic. *Global Biogeochemical Cycles*. https://doi.org/10.1029/2020GB006818

Maavara, T., Dürr, H. H., & Van Cappellen, P. (2014). Worldwide retention of nutrient silicon by river damming: From sparse data set to global estimate. *Global Biogeochemical Cycles*, 28, 842–855. https://doi.org/10.1002/2014GB004875

Maavara, T., Lauerwald, R., Regnier, P., & Van Cappellen, P. (2017). Global perturbation of organic carbon cycling by river damming. *Nature Communications*, 8, 15347. https://doi.org/10.1038/ncomms15347

Mackenzie, F. T., Lerman, A., & Andersson, A. J. (2004). Past and present of sediment and carbon biogeochemical cycling models. *Biogeosciences*, 1(1), 11–32. https://doi.org/10.5194/bg-1-11-2004

Mackenzie, F. T., Lerman, A., & Ver, L. M. B. (1998). Role of the continental margin in the global carbon balance during the past three centuries. *Geology*, 26(5), 423–426. https://doi.org/10.1130/0091-7613(1998)026%3C0423:ROTCMI%3E2.3.CO

Mackenzie, F. T., Ver, L. M., & Lerman, A. (2002). Century-scale nitrogen and phosphorus controls of the carbon cycle. *Chemical Geology*, 190(1), 13–32. https://doi.org/10.1016/S0009-2541(02)00108-0

Maerz, J., Six, K. D., Stemmler, I., Ahmerkamp, S., & Ilyina, T. (2020). Microstructure and composition of marine aggregates as co-determinants for vertical particulate organic carbon transfer in the global ocean. *Biogeosciences*, 17(7), 1765–1803. https://doi.org/10.5194/bg-17-1765-2020

Mahowald, N. M., Baker, A. R., Bergametti, G., Brooks, N., Duce, R. A., Jickells, T. D., Kubilay, N., Prospero, J. M., & Tegen, I. (2005). Atmospheric global dust cycle and iron inputs to the ocean. *Global Biogeochemical Cycles*, 19(4). https://doi.org/10.1029/2004GB002402

Mahowald, N., Jickells, T. D., Baker, A. R., Artaxo, P., Benitez-Nelson, C. R., Bergametti, G., Bond, T. C., Chen, Y., Cohen, D. D., Herut, B., Kubilay, N., Losno, R., Luo, C., Maenhaut, W., McGee, K. A., Okin, G. S., Siefert, R. L., & Tsukuda, S. (2008). Global distribution of atmospheric phosphorus sources, concentrations and deposition rates, and anthropogenic impacts. *Global Biogeochemical Cycles*, 22, GB4026. https://doi.org/10.1029/2008GB003240

Mahowald, N. M., Scanza, R., Brahney, J., Goodale, C. L., Hess, P. G., Moore, J. K., & Neff, J. (2017). Aerosol deposition impacts on land and ocean carbon cycles. *Current Climate Change Reports*, 3(1), 16–31. https://doi.org/10.1007/s40641-017-0056-z

Martinelli, L. A., Coletta, L. D., Ravagnani, E. C., Camargo, P. B., Ometto, J., Filoso, S., & Victoria, R. L. (2010). Dissolved nitrogen in rivers: Comparing pristine and impacted regions of Brazil. *Brazilian Journal of Biology*, 70, 709–722. https://doi.org/10.1590/S1519-69842010000400003

Mathis, M., Elizalde, A., & Mikolajewicz, U. (2019). The future regime of Atlantic nutrient supply to the Northwest European Shelf. *Journal of Marine Systems*, 189, 98–115. https://doi.org/10.1016/j.jmarsys.2018.10.002

Mathis, M., & Mikolajewicz, U. (2020). The impact of meltwater discharge from the Greenland ice sheet on the Atlantic nutrient supply to the northwest European shelf. *Ocean Science*, 16(1), 167–193. https://doi.org/10.5194/os-16-167-2020

Matsumoto, K., Tokos, K. S., Chikamoto, M. O., & Ridgwell, A. (2010). Characterizing post-industrial changes in the ocean carbon cycle in an Earth system model. *Tellus, Series B: Chemical and Physical Meteorology*, 62(4), 296–313. https://doi.org/10.1111/j.1600-0889.2010.00461.x

Mauritsen, T., Bader, J., Becker, T., Behrens, J., Bittner, M., Brokopf, R., Brovkin, V., Claussen, M., Crueger, T., Esch, M., Fast, I., Fiedler, S., Fläschner, D., Gayler, V., Giorgetta, M., Goll, D. S., Haak, H., Hagemann, S., Hedemann, C., ... Roeckner, E. (2013). Developments in the MPI-M Earth System Model version 1.2 (MPI-ESM 1.2) and its response to increasing CO_2. *Journal of Advances in Modeling Earth Systems*, 11, 998–1038. https://doi.org/10.1029/2018MS001400

Mauritsen, T., Bader, J., Becker, T., Behrens, J., Bittner, M., Brokopf, R., Brovkin, V., Claussen, M., Crueger, T., Esch, M., Fast, I., Fiedler, S., Fläschner, D., Gayler, V., Giorgetta, M., Goll, D. S., Haak, H., Hagemann, S., Hedemann, C., ... Schulzweida, U. (2018). *Developments in the MPI-M Earth System Model. Version 1.2 (MPI-ESM1.2) and its response to increasing CO_2*. https://doi.org/10.1029/2018MS001400

Mayorga, E., Seitzinger, S. P., Harrison, J. A., Dumont, E., Beusen, A. H. W., Bouwman, A. F., Fekete, B. M., Kroeze, C., & Drecht, G. V. (2010). Global Nutrient Export from WaterSheds 2 (NEWS 2): Model development and implementation. *Environmental Modelling & Software*, 25(7), 837–853. https://doi.org/10.1016/j.envsoft.2010.01.007

Meier, H. E. M., Eilola, K., Almroth-Rosell, E., Schimanke, S., Kniebusch, M., Höglund, A., Pemberton, P., Liu, Y., Väli, G., & Saraiva, S. (2019). Disentangling the impact of nutrient load and climate changes on Baltic Sea hypoxia and eutrophication since 1850. *Climate Dynamics*, 53(1), 1145–1166. https://doi.org/10.1007/s00382-018-4296-y

Meybeck, M. (1982). Carbon, nitrogen, and phosphorus transport by world rivers. *American Journal of Science*, 282, 401–450. https://doi.org/10.2475/ajs.282.4.401

Monsen, N. E., Cloern, J. E., Lucas, L. V., & Monismith, S. G. (2002). A comment on the use of flushing time, residence time, and age as transport time scales. *Limnology and Oceanography*, 47(5), 1545–1553. https://doi.org/10.4319/lo.2002.47.5.1545

Muller-Karger, F. E., Varela, R., Thunell, R., Luerssen, R., Hu, C., & Walsh, J. J. (2005). The importance of continental margins in the global carbon cycle. *Geophysical Research Letters*, 32(1). https://doi.org/10.1029/2004GL021346

NOAA National Geophysical Data Center. (2006). *2-minute Gridded Global Relief Data (ETOPO2) v2*. NOAA National Centers for Environmental Information. https://doi.org/10.7289/V5J1012Q

OSPAR. (2017). *OSPAR intermediate assessment: D5 - Eutrophication*. OSPAR Commission. https://oap.ospar.org/en/ospar-assessments/intermediate-assessment-2017

Pätsch, J., Burchard, H., Dieterich, C., Gräwe, U., Gröger, M., Mathis, M., Kapitza, H., Bersch, M., Moll, A., Pohlmann, T., Su, J., Ho-Hagemann, H. T. M., Schulz, A., Elizalde, A., & Eden, C. (2017). An evaluation of the North Sea circulation in global and regional models relevant for ecosystem simulations. *Ocean Modelling*, 116, 70–95. https://doi.org/10.1016/j.ocemod.2017.06.005

Paulsen, H., Ilyina, T., Six, K. D., & Stemmler, I. (2017). Incorporating a prognostic representation of marine nitrogen fixers into the global ocean biogeochemical model HAMOCC. *Journal of Advances in Modeling Earth Systems*, 9(1), 438–464. https://doi.org/10.1002/2016MS000737

Peierls, B., Caraco, N., Pace, M., & Cole, J. (1991). Human influence on river nitrogen. *Nature*, 350, 386–387. https://doi.org/10.1038/350386b0

Pershing, A., Mills, K., Dayton, A., Franklin, B., & Kennedy, B. (2018). Evidence for adaptation from the 2016 marine heatwave in the northwest Atlantic ocean. *Oceanography*, 31. https://doi.org/10.5670/oceanog.2018.213

Peters, G. P., Le Quéré, C., Andrew, R. M., Canadell, J. G., Friedlingstein, P., Ilyina, T., Jackson, R. B., Joos, F., Korsbakken, J. I., McKinley, G.

A., Sitch, S., & Tans, P. (2017). Towards real-time verification of CO_2 emissions. *Nature Climate Change*, 7(12), 848–850. https://doi.org/10.1038/s41558-017-0013-9

Poli, P., Hersbach, H., Dee, D. P., Berrisford, P., Simmons, A. J., Vitart, F., Laloyaux, P., Tan, D. G. H., Peubey, C., Thépaut, J.-N., Trémolet, Y., Hólm, E. V., Bonavita, M., Isaksen, L., & Fisher, M. (2016). ERA-20C: An atmospheric reanalysis of the twentieth century. *Journal of Climate*, 29(11), 4083–4097. https://doi.org/10.1175/JCLI-D-15-0556.1

Rabalais, N. N., Turner, R. E., & Wiseman, W. J. (2002). Gulf of Mexico Hypoxia, A.K.A. "The Dead Zone". *Annual Review of Ecology and Systematics*, 33(1), 235–263. https://doi.org/10.1146/annurev.ecolsys.33.010802.150513

Rabouille, C., Mackenzie, F. T., & Ver, L. M. (2001). Influence of the human perturbation on carbon, nitrogen, and oxygen biogeochemical cycles in the global coastal ocean. *Geochimica et Cosmochimica Acta*, 65(21), 3615–3641. https://doi.org/10.1016/S0016-7037(01)00760-8

Radach, G., & Pätsch, J. (2007). Variability of continental riverine freshwater and nutrient inputs into the North Sea for the years 1977–2000 and its consequences for the assessment of eutrophication. *Estuaries and Coasts*, 30(1), 66–81. https://doi.org/10.1007/BF02782968

Regnier, P., Friedlingstein, P., Ciais, P., Mackenzie, F. T., Gruber, N., Janssens, I. A., Laruelle, G. G., Lauerwald, R., Luyssaert, S., Andersson, A. J., Arndt, S., Arnosti, C., Borges, A. V., Dale, A. W., Gallego-Sala, A., Goddéris, Y., Goossens, N., Hartmann, J., Heinze, C., ... Thullner, M. (2013). Anthropogenic perturbation of the carbon fluxes from land to ocean. *Nature Geoscience*, 6, 597. https://doi.org/10.1038/ngeo1830

Rhein, M., Rintoul, S., Aoki, S., Campos, E., Chambers, D., Feely, R., & Wang, F. (2013). Observations: Ocean. In climate change 2013: The physical science basis. Contribution of working group I to the fifth assessment report of the Intergovernmental Panel on Climate Change. In T. Stocker, D. Qin, K. Plattner, M. Tignor, S. Allen, J. Boschung, A. Nauels, Y. Xia, V. Bex, & P. Midgley (Eds.), *Fifth assessment report of the Intergovernmental Panel on Climate Change* (pp. 255–316). Cambridge University Press.

Saba, V. S., Friedrichs, M. A. M., Antoine, D., Armstrong, R. A., Asanuma, I., Behrenfeld, M. J., Ciotti, A. M., Dowell, M., Hoepffner, N., Hyde, K. J. W., Ishizaka, J., Kameda, T., Marra, J., Mélin, F., Morel, A., O'Reilly, J., Scardi, M., Smith, W. O., Smyth, T. J., ... Westberry, T. K. (2011). An evaluation of ocean color model estimates of marine primary productivity in coastal and pelagic regions across the globe. *Biogeosciences*, 8(2), 489–503. https://doi.org/10.5194/bg-8-489-2011

Sabine, C. L., Feely, R. A., Gruber, N., Key, R. M., Lee, K., Bullister, J. L., Wanninkhof, R., Wong, C. S., Wallace, D. W. R., Tilbrook, B., Millero, F. J., Peng, T.-H., Kozyr, A., Ono, T., & Rios, A. F. (2004). The oceanic sink for anthropogenic CO_2. *Science*, 305(5682), 367–371. https://doi.org/10.1126/science.1097403

Sattar, M. A., Kroeze, C., & Strokal, M. (2014). The increasing impact of food production on nutrient export by rivers to the Bay of Bengal 1970–2050. *Marine Pollution Bulletin*, 80(1), 168–178. https://doi.org/10.1016/j.marpolbul.2014.01.017

Seitzinger, S. P., Mayorga, E., Bouwman, A. F., Kroeze, C., Beusen, A. H. W., Billen, G., Drecht, G. V., Dumont, E., Fekete, B. M., Garnier, J., & Harrison, J. A. (2010). Global river nutrient export: A scenario analysis of past and future trends. *Global Biogeochemical Cycles*, 24(4). https://doi.org/10.1029/2009GB003587

Seland, Ø., Bentsen, M., Olivié, D., Toniazzo, T., Gjermundsen, A., Graff, L. S., Debernard, J. B., Gupta, A. K., He, Y.-C., Kirkevåg, A., Schwinger, J., Tjiputra, J., Aas, K. S., Bethke, I., Fan, Y., Griesfeller, J., Grini, A., Guo, C., Ilicak, M., ... Schulz, M. (2020). Overview of the Norwegian Earth System Model (NorESM2) and key climate response of CMIP6 DECK, historical, and scenario simulations. *Geoscientific Model Development*, 13(12), 6165–6200. https://doi.org/10.5194/gmd-13-6165-2020

Shuiwang, D., Shen, Z., & Hongyu, H. (2000). Transport of dissolved inorganic nitrogen from the major rivers to estuaries in China. *Nutrient Cycling in Agroecosystems*, *57*(1), 13–22. https://doi.org/10.1023/A:1009896032188

Six, K. D., & Maier-Reimer, E. (1996). Effects of plankton dynamics on seasonal carbon fluxes in an ocean general circulation model. *Global Biogeochemical Cycles*, *10*, 559–583. https://doi.org/10.1029/96GB02561

Sprague, L. A., Hirsch, R. M., & Aulenbach, B. T. (2011). Nitrate in the Mississippi river and its tributaries, 1980 to 2008: Are we making progress? *Environmental Science & Technology*, *45*(17), 7209–7216. https://doi.org/10.1021/es201221s

St-Laurent, P., Friedrichs, M. A. M., Najjar, R. G., Martins, D. K., Herrmann, M., Miller, S. K., & Wilkin, J. (2017). Impacts of atmospheric nitrogen deposition on surface waters of the western north Atlantic mitigated by multiple feedbacks. *Journal of Geophysical Research: Oceans*, *122*(11), 8406–8426. https://doi.org/10.1002/2017JC013072

Stumm, W. (1973). The acceleration of the hydrogeochemical cycling of phosphorus. *Water Research*, *7*(1), 131–144. https://doi.org/10.1016/0043-1354(73)90158-9

Sylvan, J. B., Dortch, Q., Nelson, D. M., Maier Brown, A. F., Morrison, W., & Ammerman, J. W. (2006). Phosphorus limits phytoplankton growth on the Louisiana shelf during the period of hypoxia formation. *Environmental Science & Technology*, *40*(24), 7548–7553. https://doi.org/10.1021/es061417t

Takahashi, T., Broecker, W. S., & Langer, S. (1985). Redfield ratio based on chemical data from isopycnal surfaces. *Journal of Geophysical Research: Oceans*, *90*(C4), 6907–6924. https://doi.org/10.1029/JC090iC04p06907

Terhaar, J., Orr, J. C., Ethé, C., Regnier, P., & Bopp, L. (2019). Simulated Arctic ocean response to doubling of riverine carbon and nutrient delivery. *Global Biogeochemical Cycles*, *33*(8), 1048–1070. https://doi.org/10.1029/2019GB006200

Thomas, H., Bozec, Y., de Baar, H. J. W., Elkalay, K., Frankignoulle, M., Schiettecatte, L.-S., Kattner, G., & Borges, A. V. (2005). The carbon budget of the North Sea. *Biogeosciences*, *2*, 87–96. https://doi.org/10.5194/bg-2-87-2005

Tjiputra, J. F., Schwinger, J., Bentsen, M., Morée, A. L., Gao, S., Bethke, I., Heinze, C., Goris, N., Gupta, A., He, Y., Olivié, D., Seland, Ø., & Schulz, M. (2020). Ocean biogeochemistry in the Norwegian Earth System Model version 2 (NorESM2). *Geoscientific Model Development Discussions*, *2020*, 1–64. https://doi.org/10.5194/gmd-2019-347

Tseng, C.-M., Liu, K.-K., Gong, G.-C., Shen, P.-Y., & Cai, W.-J. (2011). CO_2 uptake in the East China Sea relying on Changjiang runoff is prone to change. *Geophysical Research Letters*, *38*(24). https://doi.org/10.1029/2011GL049774

Turner, R. E., Rabalais, N. N., Justic', D., & Dortch, Q. (2003). Global patterns of dissolved N, P and Si in large rivers. *Biogeochemistry*, *64*(3), 297–317. https://doi.org/10.1023/A:1024960007569

Van Bennekom, A. J., Gieskes, W. W. C., Tijssen, S. B., Cole, H. A., & Smith, J. E. (1975). Eutrophication of Dutch coastal waters. *Proceedings of the Royal Society of London. Series B. Biological Sciences*, *189*(1096), 359–374. https://doi.org/10.1098/rspb.1975.0062

Van Drecht, G., Bouwman, A. F., Boyer, E. W., Green, P., & Siebert, S. (2005). A comparison of global spatial distributions of nitrogen inputs for nonpoint sources and effects on river nitrogen export. *Global Biogeochemical Cycles*, *19*(4). https://doi.org/10.1029/2005GB002454

Ver, L. M. B., Mackenzie, F. T., & Lerman, A. (1999). Carbon cycle in the coastal zone: Effects of global perturbations and change in the past three centuries. *Chemical Geology*, *159*(1), 283–304. https://doi.org/10.1016/S0009-2541(99)00042-X

Wang, J., Yan, W., Chen, N., Li, X., & Liu, L. (2015). Modeled long-term changes of DIN:DIP ratio in the Changjiang River in relation to Chl-α and DO concentrations in adjacent estuary. *Estuarine, Coastal and Shelf Science*, *166*, 153–160. https://doi.org/10.1016/j.ecss.2014.11.028

Whitehead, P. G., Sarkar, S., Jin, L., Futter, M. N., Caesar, J., Barbour, E., Butterfield, D., Sinha, R., Nicholls, R., Hutton, C., & Leckie, H. D. (2015). Dynamic modeling of the Ganga river system: Impacts of future climate and socio-economic change on flows and nitrogen fluxes in India and Bangladesh. *Environmental Science: Processes & Impacts*, *17*(6), 1082–1097. https://doi.org/10.1039/C4EM00616J

Yang, S., & Gruber, N. (2016). The anthropogenic perturbation of the marine nitrogen cycle by atmospheric deposition: Nitrogen cycle feedbacks and the ^{15}N Haber-Bosch effect. *Global Biogeochemical Cycles*, *30*(10), 1418–1440. https://doi.org/10.1002/2016GB005421

Zhang, J., Guo, X., & Zhao, L. (2019). Tracing external sources of nutrients in the East China Sea and evaluating their contributions to primary production. *Progress in Oceanography*, *176*. https://doi.org/10.1016/j.pocean.2019.102122

SUPPORTING INFORMATION

Additional supporting information may be found online in the Supporting Information section.